2017

Three Segment Adaptive Power Electronic Compensator for Non-periodic Currents

Amin Ghaderi
University of South Carolina

Three Segment Adaptive Power Electronic Compensator for Non-periodic Currents

by

Amin Ghaderi

Bachelor of Science
University of Tehran 2008

Master of Science
Iran University of Science and Technology 2011

Submitted in Partial Fulfillment of the Requirements

for the Degree of Doctor of Philosophy in

Electrical Engineering

College of Engineering and Computing

University of South Carolina

2017

Accepted by:

Herbert L. Ginn, Major Professor

Andrea Benigni, Committee Member

Bin Zhang, Committee Member

Abdel-Moez E. Bayoumi, Committee Member

Cheryl L. Addy, Vice Provost and Dean of the Graduate School

Dedication

To my parents, my wife, and my sisters.

Acknowledgments

I would like to express my great appreciation to all of those who put time and energy to help, support, and guide me. A special thanks go to my advisor, Dr. Herbert Ginn who patiently guided me along in my studies and research, supported me to attend several conferences and presentations, and helped me in the arduous process of completing this dissertation document. He has set an example of excellence as a researcher, mentor, instructor, and role model.

I also would like to thank Dr. Yong-June Shin who gave me the opportunity to study at the University of South Carolina and taught me the fundamentals of research.

I would additionally like to thank Drs. Andrea Benigni, Bin Zhang, and Abdel-Moez Bayoumi for participating on my dissertation committee and mentoring me in the formative stages of my dissertation.

I would like to thank the members of the different research groups in Department of Electrical Engineering at the University of South Carolina, including Hossein Ali Mohammadpour, Moinul Islam, Mohammed Hassan, David Coats, Gholamreza Dehnavi, Soheila Eskandari, Hossein Banjinajar, Maryam Nasri, Hessameddin Abdollahi, Qui Dang, Cuong Nguyen, Patrick Mitchell, Rishad Hossain, Ryan Lukens, Aaron De La O, Sean Borgsteede, and MD Multan .

I would like to thanks all my friends in Columbia, South Carolina, who have been like a family to me. Last, but not least, I would like to thank my wife who has patiently supported me throughout my study, to my parents who dedicated their lives to the well-being of their children, and to my sisters.

Abstract

In this dissertation, a new technique is proposed for the compensation of non-periodic load current. The method provides control references for three co-located devices, each corresponding to one moving calculation window and one decomposed part of the compensated current. They are slow compensator with high power rating, large calculation window, and low switching frequency; fast compensator with lower power rating, shorter calculation window, and higher switching frequency; and the reactive compensator which is an ordinary static VAR compensator (SVC). To improve the flexibility of the technique, a fuzzy based adaptive window is proposed for the slow compensator to find the optimum window for different load characteristics. Moreover, three power quality criteria are proposed specifically for the non-periodic current compensation, namely, time-frequency distortion index, modulation index, and high frequency distortion index. The method is verified using both simulation and real-time implementation. First, the proposed method is verified in simulation using real-world data acquired from a local steel mill. Second, it is validated using a real-time controller-in-the-loop implementation. The proposed compensation approach demonstrates high flexibility and effectiveness in increasing power quality under various non-periodic load conditions. Finally, some practical aspects of the implementation of a three-part compensator including cost analysis are presented.

Table of Contents

List of Tables

List of Figures

Chapter 1

Introduction

Current distortion has a harmful effect on both distribution system equipment and on loads that the system supplies. Because of this, current distortion is a main cause of supply quality degradation. Furthermore, current distortion increases the root mean square value of current without increasing energy transmission. Thus, it creates increased losses during transmission of energy as well as requiring higher ratings of distribution system equipment. Therefore, it is necessary to reduce current distortion for the same reasons as for reactive current, as well as to reduce the other harmful effects. If distortion exceeds some limits, then equipment is needed for its suppression. "Compensator" is a term used for the equipment that mitigates the effect of power quality degrading loads. There are numerous types of devices and strategies available for the compensation of distorted but periodic currents from harmonic generating loads. However, although non-periodic loads, result in similar harmful effects, there has been very limited research on how to compensate them. The focus of this research is to combine the recent advances in power electronics and signal processing to manage and compensate non-periodic loads.

In this chapter, different some key concepts related to compensation are discussed. These concepts are (1) power quality, its issues, and indices, (2) power quality improving devices (compensators), (3) power theories, (4) time-frequency distribution, (5) and non-periodic loads.

1.1 Power Quality (PQ)

In general, a power system quality disturbance is defined as " Any power problem manifested in voltage, current, or frequency deviations that results in failure or misoperation of customer equipment" [1]. We can add to this definition the problems that result in a decrease in the efficiency of the power systems. PQ is, therefore, defined as the absence or limited presence of power quality disturbances. Keeping the quality of power within the acceptable range has been one of the most challenging tasks of the utilities and device manufacturers. Especially, by the recent large increase in non-linear loads (power electronics based) and grid-connected distributed generation the PQ issues been worsened. It is shown that the keyword "Distributed Generation" is the fifth most used phrase in articles regarding the power quality [2].

The power quality could be seen from two aspects, the from the utility side, and from the costumer side. First, the utility is responsible for providing a supply voltage which is balanced, constant, sinusoidal, and with a fixed frequency (60 Hz in the United States). However, a little deviation from this condition is also acceptable by the standards. Improving this "voltage quality (VQ)" is the responsibility of the utility companies, and remarkable deviation from this power quality would result in failure and mal-operation of power systems and the loads. Some examples of such power quality disturbance are voltage sag [3], voltage swell [4], voltage interruption[5], voltage harmonic [6], voltage imbalance [7], voltage flicker [8], voltage transient [9], and frequency deviation[10].

The second perspective of the power quality is the consumer side. The customer is responsible for drawing a current waveform which has the same shape as the voltage waveform with possibly different magnitude. In other words, for a system with a sinusoidal voltage supply, the current waveform of the load should have the same phase angle and frequency to assure acceptable power quality (constant equivalent conduc-

tance and zero equivalent susceptance). Any load that does not have balanced pure resistive characteristics is considered a PQ degrading load. Though small deviation from this condition is acceptable, larger variation results in a decrease of the power system efficiency. This lower efficiency is the product of several factors; increase in the power loss, elevation of the source current RMS, and elevation of the line voltage distortion. As a result, the customers with unacceptable "current quality (CQ)" will end up paying penalties to the utility. Some example of the CQ disturbance are load reactive power [11], load harmonic [12], unbalance load [13], load inter-harmonic [14].

It is noted that CQ disturbances could lead to VQ disturbances and vice versa. For example, large load current drawn from a non-linear load would result in a significant voltage drop on the line impedance, which in turn results in distorted voltage waveform. On the other hand, also, the distorted voltage on a balanced resistive load would also lead to current waveform distortion. Therefore, it is the responsibility of the utility to provide voltage supply with acceptable VQ and then the responsibility of the consumers to maintain acceptable CQ. It is noted that the primary purpose of this dissertation is the improvement of the CQ disturbances which are the byproduct of large steel mills. However, in the last part of the dissertation, a possible VQ disturbance improvement for the microgrids (MG) is also proposed.

1.1.1 Power Quality Indices

In general, the indices used to evaluate the quality of power are categorized into three groups, namely, waveform distortion indices, equivalent susceptance indices, and sequence indices.

The first group of PQ indices is waveform distortion indices that are used for both VQ and CQ disturbance evaluation. The most famous index in this group is the "Total Harmonic Distortion (THD)" index which is used to quantify the level of harmonic distortion (existence of sinusoidal components whose frequency is multiple integers

of the fundamental frequency). THD is calculated using the following equation:

$$THD = \sqrt{\frac{\sum_{n=0}^{\infty} \quad X(n\omega_0)^2 - X(\omega_0)^2}{X(\omega_0)^2}}\% \tag{1.1}$$

where X is the quantity of interest (current or voltage), ω_0 is the fundamental frequency in rad/s, and n is the harmonic order. Other indices in this category are crest factor [15], notch area (and notch depth) [16], and instantaneous distortion energy ratio [17].

The second group of power quality criteria is the equivalent susceptance indices. For a load to receive the required active power with the highest efficiency, it is necessary that its equivalent susceptance is equal to zero. It is noted that the equivalent susceptance (B_e) is proportionally related to the reactive power consumption ($Q_L = B_e \times V^2$). The most popular power quality index in this category is the power factor (PF) which is calculated as follows:

$$PF = \quad \frac{P}{S} = cos(\varphi) \tag{1.2}$$

where P is the load active power, S is the load apparent power, and ϕ is the phase displacement between voltage and the current waveform. It is noted that this definition holds meaning only for sinusoidal and balanced systems [18]. Other indices in this group are displacement factor, interactive power transfer factor, and reactive power transfer factor [19]. It is noted that this group of power quality indices is mainly related to CQ disturbances.

The third group of power quality criteria, sequence indices, are evaluating the level of balance in the power system and loads. Therefore, these indices are also working for both CQ and VQ disturbances. They are called sequence indices since any imbalance in power system could be reflected in the existence of negative and zero sequence components of voltage or current [20]. The most popular power quality factor in this group is the unbalanced factor (UF) which is calculated as follows:

$$UF_X = \frac{X^N}{X^P} \tag{1.3}$$

where X is the quantity of interest, N superscript demonstrates the negative sequence, and P superscript demonstrates the positive sequence. some other indices in this group are $VUNB$ and $IUNB$ proposed in [21].

Although the existing PQ indices are capable of describing the level of PQ disturbance in most of the normal loads and network, for some especial cases, such as for the loads from steel mills, these PQ indices lose their meaning. Chapter 2 is dedicated to the discussion on the difference between non-periodic loads (such as steel mills) and periodic loads. Moreover, a new set of PQ indices is proposed that are capable of evaluating this situation.

1.2 Power Quality Improving Devices

Various technologies have been developed to address the PQ disturbances and bring the power system state back within the acceptable PQ indices. These devices are divided into two basic categories, passive devices, and active devices. Passive devices are always pre-designed based on the power system condition to mitigate some PQ disturbances partially. Active devices, on the other hand, adaptively modify their behavior to comply with the changes in the system configuration, loading, or generation. The power quality improving devices are called compensators. In this section passive and active compensators are introduced in more details.

1.2.1 Passive Compensators

Passive compensators could be divided into four categories: (1) power factor correction devices, (2) harmonic reduction devices, (3) voltage profile improvement [22].

The first group of passive compensators, power factor correction devices are mainly

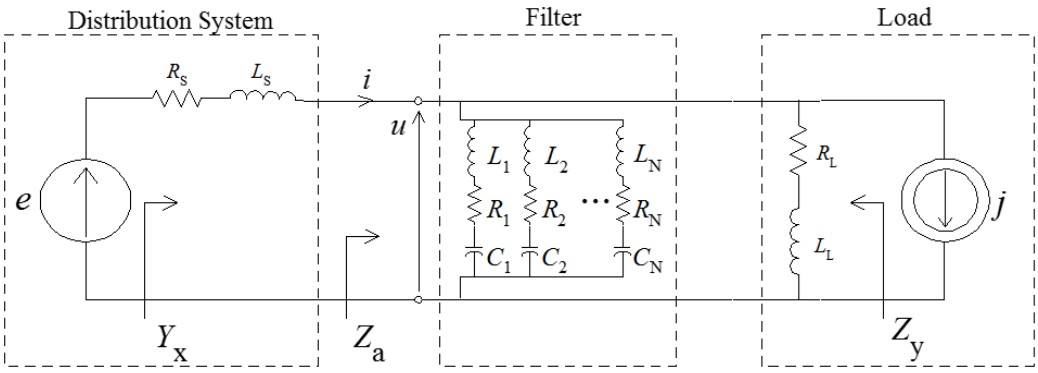

Figure 1.1: Typical structure of a passive filter.

shunt capacitors and shunt inductors used to improve the CQ of the load. They are designed to generate (or consume) the reactive power that the load consumes (or generates). The rating and values of these components are pre-calculated, and they are installed, usually, at the load terminal. The problem with these compensators is their unresponsiveness to the load changes and system changes [23]. Moreover, they might result in resonance with the line impedance.

The second group of passive compensators, harmonic reduction devices (also known as passive filters), are mainly shunt tuned LC filters that are designed to make an extremely large conductance path for current harmonics. Fig. 1.1 demonstrates the equivalent circuit for one phase of a passive filter connected to a harmonic generating load in the distribution system. These filters require one series RLC branch for each harmonic are eliminating. Though these devices are cheap and reliable for most periodic loads, they tend to become ineffective for loads with more complicated harmonic patterns (such as non-periodic loads).

The third group of passive compensator is voltage profile improvement devices. These devices are (switched) capacitor- and inductor banks located in both distribution and transmission network to compensate for loads with large reactive power transactions and Ferranti effect [24]. Both of these situations result in exceeding the voltage magnitude beyond acceptable voltage level. These compensators can be shunt or in series with the lines.

1.2.2 Active Compensators

Active compensators are capable of adaptively track the PQ disturbances. Therefore, they are responsive to the change in loads and network configuration. These compensators are divided into three groups: Static VAR Compensators (SVCs), Static Series Compensators, and Switching Compensators.

The first class of active compensators, SVCs are adaptive susceptances. They use a combination of passive elements (inductors, capacitors, and resistors) and active devices (Thyristors) to form a controlled susceptance. SVCs are mainly used to compensate for reactive power generation/consumption. Moreover, more heuristics structures of SVCs can also compensate unbalanced power. The main drawback of the SVCs is the fact that the use of switching components results in the generation of harmonic current, which in some cases are fairly large. Fig. 1.2 demonstrates three popular structures of the SVC. In this dissertation, we perform a cost analysis to explore the most optimal structure for the development of our technique.

The first structure of SVC, FC-TCR (fixed capacitor- thyristor controlled reactor), shown in Fig. 1.2a is capable of compensating reactive power [25]. However, it generates current harmonics of the order $6k \pm 1$ multiples of the fundamental frequency. Moreover, this compensator is incapable of compensating the unbalanced power. The second structure, 12-pulse FC-TCR is shown in Fig. 1.2b. This device consists of one $Y - Y$ and one $Y - \Delta$ transformer that together reduces the harmonic content of the reactive compensator to $12k \pm 1$ multiples of the fundamental frequency [25]. However, similar to the basic FC-TCR, 12-pulse FC-TCR is incapable of compensating the unbalanced power. The third structure, adaptive balancing compensator, is shown in Fig. 1.2c. This configuration is an extension of the FC-TCR that is also capable of compensating the unbalanced part of the current [26]. However, since for the compensation of unbalance power the value of each phase to phase impedance

should be different, the triple-nth harmonics generated by the TCR branch could not circulate inside the delta connected compensator and will be injected into the line. Therefore, although this compensator is capable of compensating the unbalanced power, it generates and injects $2k \pm 1$ multiples of the fundamental frequency to the grid.

The second class of active compensators is Static Series Compensators. These compensators are mainly used to mitigate the subsynchronous resonance [27, 28], controlling the transmitted power [29], and preventing loop flows.

The last class of active compensators, switching compensators (also known as active filters) are controlled current sources. The basic structure of an active filter is shown in Fig. 1.3. When a voltage source converter is accompanied by a proper control algorithm, it could behave as a controlled current source. Therefore, assuming enough bandwidth and rating, it would be able to compensate harmonics, reactive current, and unbalance current. Therefore, if this current source is controlled to generate the distortion part of the current in the opposite direction, active filter compensates the load.

The most important subsystem within the control structure of an active filter is the "reference signal generation" block which is responsible for calculating the distortion part of the current. Various "Power Theories" have been developed to calculate this distortion part of the current, which will be discussed briefly in Section 1.3 below. It is noted that the main focus of this dissertation is to develop an appropriate reference signal generation block, that is capable of compensating different part of the current waveform of the non-periodic loads.

1.3 Power Theories

Power theories are mathematical techniques used for decomposing the current waveform into various components, based on the applications, requirement, and avail-

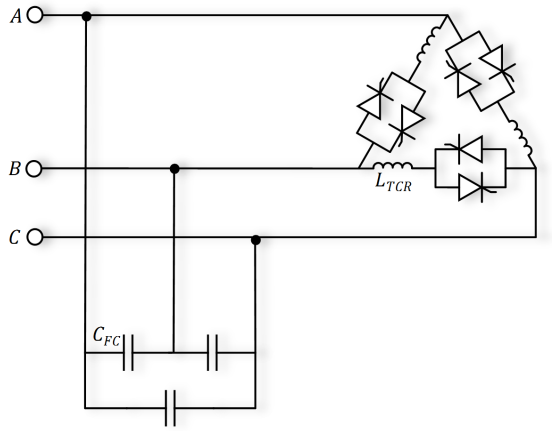

(a) Fixed capacitor thyristor controlled reactor (FC-TCR)

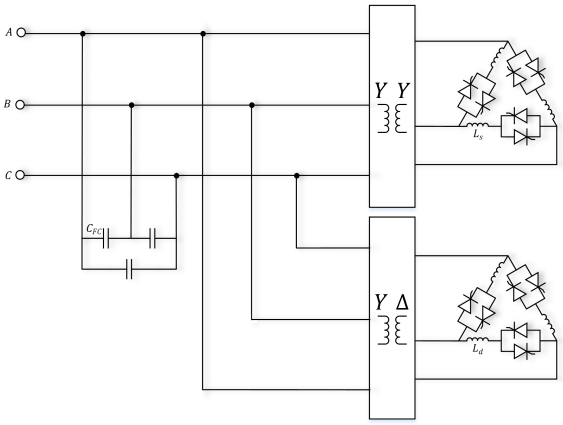

(b) Fixed capacitor 12-pulse thyristor controlled reactor.

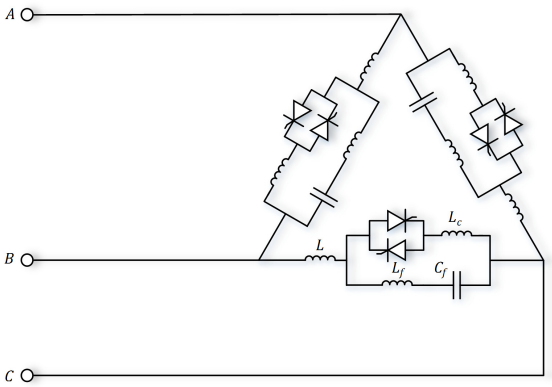

(c) Adaptive balancing compensator.

Figure 1.2: Popular structures of SVCs.

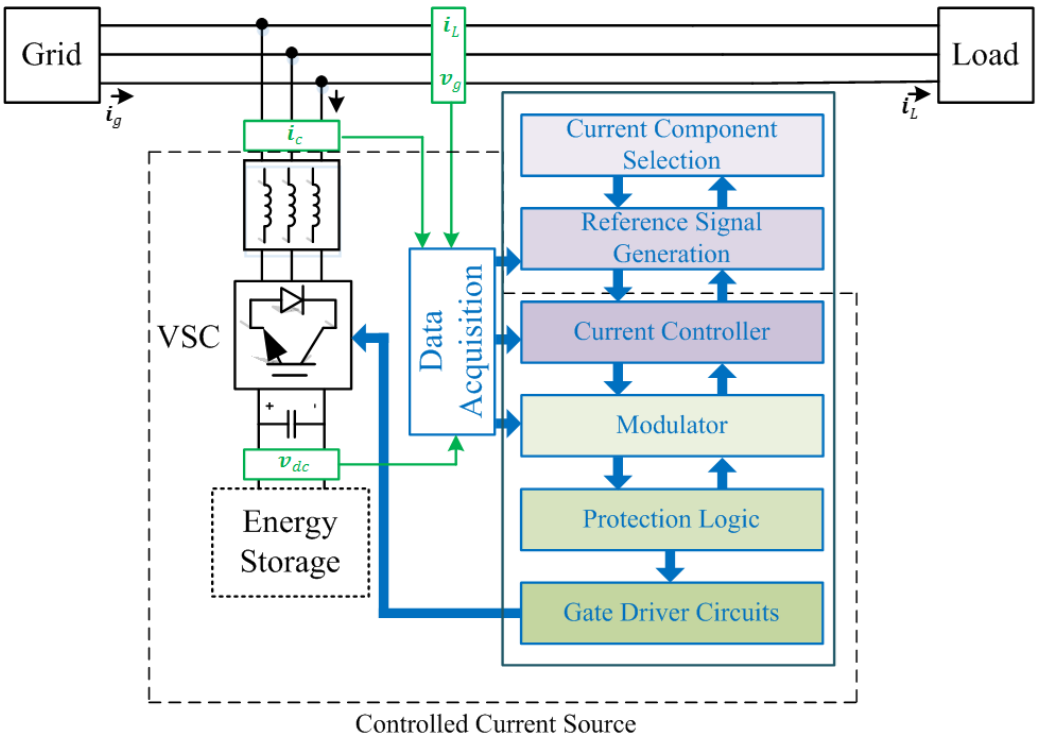

Figure 1.3: Typical structure of an active filter.

able technologies. These current (power) components could be utilized for different applications, such as energy metering, compensation, performance evaluation, and system design [18]. Moreover, depending on the design requirement, and available technologies, different power theories might be suitable for various applications. In this section, the main power theories developed for the application purposes are discussed.

References [30] and [31] provide comprehensive reviews on the power theories utilized by different active filters. Morsi et al. [18], also, investigate the power theories using bottom-up and top-down approaches. These power theories are placed into three subcategories, namely, time-domain based methods, frequency domain based method, and hybrid time-frequency domain-based methods.

1.3.1 Time-domain power theories

The time-domain based power theories decompose the current waveform into its orthogonal components without using mapping the power components (voltage and current) to any other domains (e.g. frequency, time-frequency, wavelet). Most well-known time domain power theories are Fryze power theory and instantaneous pq power theory.

Fryze theory takes advantage of the fact that the only part of the current waveform which is contributing to the power transfer has the same shape as the voltage waveform [32]. Therefore, this theory simply divides the load current into two parts, the active current, which is responsible for the power transfer, and the non-active part which does not contribute to the transfer:

$$p(t) = v(t)i_L(t) \Rightarrow instantanous\ power \tag{1.4}$$

$$P = \frac{1}{T}\int_0^T p(t)dt \Rightarrow active\ power \tag{1.5}$$

$$G_e = \frac{P}{{V_{RMS}}^2} \Rightarrow equivalent\ conductance \tag{1.6}$$

$$i_a(t) = G_e v(t) \Rightarrow active\ current \tag{1.7}$$

The remaining part of the current is named non-active current ($i_{na}(t) = i_L(t) - i_a(t)$). This part does not contribute to the power transfer and needs to be compensated using the active filter. It is noted that the advantage of the Fryze theory is its simplicity. However, using Fryze theory, the optimum utilization of bandwidth and rating of the active filter and also the integration of active filter with other devices are not possible.

The second popular time-domain power theory is the instantaneous pq power theory [33]. This theory has been widely used for the control of power converter due to its simplified design and high-speed [34].This power theory first transfers the three-phase quantities (voltage and current) into the rotating frame using the Park

transform.

$$v_{\alpha\beta 0} = T v_{abc} \tag{1.8}$$

$$i_{\alpha\beta 0} = T i_{abc} \tag{1.9}$$

where v and i are voltage and current vector, respectively. abc and $\alpha\beta 0$ subscript demonstrate the vector in the abc and rotating domain, respectively. T is the Park domain mapping matrix calculated as follows:

$$T = \sqrt{\frac{2}{3}} \begin{bmatrix} \cos(\theta) & \cos(\theta - \frac{2\pi}{3}) & \cos(\theta + \frac{2\pi}{3}) \\ \sin(\theta) & \sin(\theta - \frac{2\pi}{3}) & \sin(\theta + \frac{2\pi}{3}) \\ \frac{\sqrt{2}}{2} & \frac{\sqrt{2}}{2} & \frac{\sqrt{2}}{2} \end{bmatrix} \tag{1.10}$$

where θ is the rotation angle of the rotating frame.

After mapping the quantities into the rotating frame, the instantaneous powers are calculated as follows:

$$\begin{bmatrix} p_0 \\ p \\ q \end{bmatrix} = M \begin{bmatrix} i_0 \\ i_\alpha \\ i_\beta \end{bmatrix} \tag{1.11}$$

$$M = \sqrt{\frac{2}{3}} \begin{bmatrix} v_0 & 0 & 0 \\ 0 & v_\alpha & v_\beta \\ 0 & v_\beta & -v_\alpha \end{bmatrix} \tag{1.12}$$

where p is known as instantaneous real power and consists of constant ($\bar{p}$) and osculating ($\tilde{p}$) parts; q is known as instantaneous imaginary power which also consists of constant and oscillatory parts ($q = \bar{q} + \tilde{q}$); and finally, p_0 is known as the instantaneous zero-sequence power ($p_0 = \bar{p_0} + \tilde{p_0}$).

It is shown that among these six power components ($\bar{p}$, $\bar{q}$, $\bar{p_0}$, and $\tilde{p}$, $\tilde{q}$, $\tilde{p_0}$), only constant part of the real power contributes to the power transfer ($\bar{p}$). Therefore, the reference signal generating block calculates the current waveform corresponding

to the five power components that are not contributing to the power transfer. The voltage source converter generates this value to annihilate the distortion part of the current. The reference current is calculated as follows:

$$i_{\alpha\beta 0}{}^{*} = \begin{bmatrix} i_0 \\ i_\alpha \\ i_\beta \end{bmatrix} = M^{-1} \begin{bmatrix} \tilde{p}_0 \\ \tilde{p} \\ q \end{bmatrix} \tag{1.13}$$

$$i_c{}^{*} = T^{-1} i_{\alpha\beta 0}{}^{*} \tag{1.14}$$

Though the instantaneous pq power theory is simple and fast, it loses its reliability for compensating the various abnormal loadings, such as non-periodic loads.

1.3.2 Frequency-domain power theories

The second class of power theories are frequency-domain based. They require the preprocessing of the data and mapping from the time domain to the frequency domain. Th most popular power theory in this class is the Current Physical Component theory. In this technique, the non-active part of the current is further decomposed into four parts, reactive, unbalanced, scattered, and generated [35]. It is suggested that each part of the non-active current can be compensated separately. The technique is similar to the Fryze theory up to the point that it calculates the active current. The remaining current are calculated as follows:

$$i_r = \sqrt{2} Re\{\sum_{n\in N} jB_{en} U_n e^{jn\omega_1 t}\} \Rightarrow reactive\ current \tag{1.15}$$

$$i_u = \sqrt{2} Re\{\sum_{n\in N} AU^{\#} e^{jn\omega_1 t}\} \Rightarrow unbalanced\ current \tag{1.16}$$

$$i_s = \sqrt{2} Re\{\sum_{n\in N} (G_e - G_n) U_n e^{jn\omega_1 t}\} \Rightarrow scattered\ current \tag{1.17}$$

$$i_g = \sum_{h\in(N_i \cap \bar{N}_v)} i_h \Rightarrow generated\ current \tag{1.18}$$

where G_e is the load equivalent conductance, U is the voltage phasor, $U^{\#}$ is the voltage phasor transpose, B_{en} is the equivalent susceptance of each harmonic, A is the unbalanced admittance, G_n is the harmonic equivalent conductance. N is the set of harmonic orders in voltage and current, N_i is the set of harmonic orders in current, and N_v is the set of harmonic orders in voltage.

The decomposition of the current waveform into several components is very helpful for sharing the rating and bandwidth between different compensators. However, for some abnormal loading cases, such as non-periodic loads, the definition of frequency components using solely FFT is not efficient anymore. The reason is that these loads do not only contain multiple integers of the fundamental frequency components. Therefore, the CPC theory would become ineffective in such cases. Moreover, in the case that the voltage waveform is more distorted than the current waveform, the CPC theory would increase the line current distortion.

1.3.3 Hybrid-domain power theories

Hybrid time-frequency algorithms combine time and frequency domain approaches. Czarnecki et. al [36] proposed a hybrid active filter that consists of a frequency domain method for the compensation of reactive powers and a time-domain method for the compensation of non-periodicity. Such techniques are, however, more complex, not verified for non-periodic current compensation, and may increase the line current THD in the case of a highly distorted supply voltage.

1.4 Time-Frequency Analysis (TFA)

TFA was motivated by the need to describe non-stationary signals, where Fourier transform proves ineffective. Non-stationary signals are the ones whose frequency spectrum varies over time, such as non-periodic load current. Several time-frequency

representation methods are designed to mathematically describe these signals, namely short time Fourier transform (STFT), Wigner-Ville distribution (WVD), and Choi-Williams distribution (CWD) [37]-[38]. To systematically design proper time-frequency distribution (TFD), Cohen generalization of the quadratic TFDs is used [37]. Cohen proved that one can relate the desirable properties of TFDs to constraints on its kernel:

$$TFD_s(t,\omega) = \frac{1}{4\pi^2}\iiint_{-\infty}^{\infty} IAC_s(u,\tau)\phi(\theta,\tau) \times e^{-j\theta t - j\tau\omega + j\tau u} d\theta d\tau du \quad (1.19)$$

where $\phi(\theta,\tau)$ is a two dimensional function (in Doppler-lag domain), called *kernel* and TFD_s is the time-frequency distribution of the signal. The constant time cross section of time frequency distribution ($TFD(t_0,\omega)$) represents the frequencies available at time t_0, and its frequency cross section ($TFD(t,\omega_0)$) represents the times when frequency ω_0 occurred. And IAC_s is the *instantaneous auto-correlation* of the signal $s(t)$, respectively. IAC_s is defined in Eq.(2.2).

$$IAC_s(t,\tau) = s^*(t-\tau/2)s(t+\tau/2) \quad (1.20)$$

The desirable properties of TFD and their constraints are defined as follows:

Time Marginal

Integration of the TFD over frequency gives the *"Instantaneous Power"* ($|s(t)|^2$):

$$\int_{-\infty}^{\infty} TFD_s(t,\omega)d\omega = |s(t)|^2 \Longleftrightarrow \phi(\theta,0) = 1 \quad (1.21)$$

Frequency Marginal

Integration of the TFD over time gives the *"Energy Spectrum"* ($|S(\omega)|^2$):

$$\int_{-\infty}^{\infty} TFD_s(t,\omega)dt = |S(\omega)|^2 \Longleftrightarrow \phi(0,\tau) = 1 \quad (1.22)$$

Global Energy

Integration of the TFD over the entire time-frequency plane yields the *"Signal Energy" (E_S)*:

$$\int_{-\infty}^{\infty}\int_{-\infty}^{\infty} TFD_s(t,\omega)dtd\omega = E_s \Longleftrightarrow \phi(0,0) = 1 \tag{1.23}$$

Reduced Interference

Due to the bi-linearity of the IAC, introducing *"artifacts"* (interference) is inevitable in generating TFDs. If the kernel has low pass filter characteristic in Doppler-lag domain (θ, τ), the interference could be reduced.
Since the disturbances in power systems are characterized by the presence of multiple frequency components over a short duration of time, keeping high time-frequency resolution, while avoiding artifacts is of great significance in their analysis [39].

Although WVD satisfies the first three constraints ($\phi(\theta, \tau) = 1$), a large proportion of interference could result in a poor interpretation of a signal. However, in the case of analyzing non-periodic current, since it is the energy of harmonics in different time-windows and frequency windows that are important, the reduced interference requirement could be waived. Therefore, for the analysis of the non-periodic load current, the WVD is chosen.

1.5 Non-periodic Load

In general, any power system quantity (voltage, current) whose frequency content is not integer multiples of the system supply frequency (i.e. 50 Hz, 60 Hz) is considered a non-periodic quantity [40]. The time duration of the non-periodicity could be from a fraction of one period of the power system frequency up to a steady state component of the current or voltage [36].

Non-periodicity in a power system shall not be confused with the mathematical meaning of non-periodicity. In the mathematical sense, a signal is considered non-periodic if it does not have a complete pattern within a measurable constant time frame. To reconcile the definition of the non-periodic signal in power systems and mathematics, Czarnecki [36] proposed a classification of the waveforms based on their periodicity, as it relates to the power system generators, namely, co-periodics, non-coperiodics, and quasi-periodics. A co-periodic quantity has an integer multiple of the power system frequency. On the contrary, a non-coperiodic quantity is a periodic or non-periodic waveform that does not have the same period of the power system generators or any of its multiples. If the non-coperiodic current has a small time duration and small magnitude comparing to the fundamental component of the signal, it is called quasi-periodic. The frequency spectrum of a quasi-periodic current, though continuous, is located in the sub-band neighborhood of the fundamental frequency (and its multiples) [41]. In this work when the term "non-periodic" is used, it means non-coperidoic.

Non-periodic current could be the result of various loads, such as cyclo-converters, welders, arc furnaces, adjustable speed drives [42]. The harmful impacts of the non-periodic currents are similar to those of harmonic loads, such as contribution to power loss, elevation of the source current RMS, interference with the local sensitive loads, elevation of the line voltage distortion, and interference with measurement devices [43].

Two widely used devices for load current compensation are active filters and passive filters [36]. Passive filters, though straightforward and inexpensive as compared to active filters, may bring a strong possibility of the amplification of inter-harmonics noise components of the current, which makes them not practically applicable for non-periodic load compensation. Therefore, active filters (switching compensators) are necessary for the compensation of such loads.

Time-domain based approaches are mostly originated from the Fryze power theory [32]- [44], instantaneous p-q theory [45, 46, 34] , and synchronous d-q frame theory [47]. In [48] and [49] an extension of Fryze power theory, and instantaneous power theory is utilized for the compensation of non-periodic current. The time-domain based techniques have the advantage of being simple and instantaneous under some specific conditions.

The second group of power theories, frequency domain approaches, are based on the Fourier transform or Kalman filtering of the current or voltage waveforms. In [50], Czarnecki proposed a frequency based method to decompose the load current into active, reactive, scattered, and generated current. Unlike the time-domain approaches, frequency based methods are more easily tailored to compensation objectives. However, they are not instantaneous, and they are more complex due to the necessity of FFT calculation of each harmonic.

1.5.1 Existing Techniques for Non-periodic Current Compensation

Compensation using Fryze theory

One of the earliest power theory to describe the power flow and decomposing the current waveform into orthogonal components is proposed by Fryze in [32]. In fact, the first time the term "power theory" is utilized was in that article. Fryze power theory decomposes the current waveform into active and non-active components; where the active component is the part of the current which is responsible for power transmission, and the non-active component is any part of the current that does not contribute to the power transfer and need to be compensated. Fryze theory has been used for different applications such as reactive current compensation, harmonic current compensation, and subharmonic current compensation.

In [48], Fryze theory is proposed for the compensation of non-periodic load current. This technique considers all the non-periodicity, harmonics, reactive current, and imbalance current as a residual non-active current. However, the feasibility of a device that is capable of such compensation is not discussed. Moreover, the proposed technique utilizes an arbitrary averaging window length for the calculation of reference current. The dissertation suggests a trade-off between averaging window length and the cost of the compensator.

Compensation using pq theory

The instantaneous pq theory, also known as instantaneous active and reactive power theory, is first proposed by Akagi in 1983 [33]. The pq theory performs a Clark transformation of current and voltage waveforms to define "instantaneous" active (p) and reactive (q) powers, and subsequently reactive and active current. pq theory has been widely used in the compensation of power quality degrading events, such as non-linear loads, imbalance loads, and systems with non-sinusoidal voltage supply [34, 51].

In [45], the pq theory is proposed for the compensation of non-periodic loads. In this technique, an integrator with "averaging time tending to infinity" is used. Moreover, it is mentioned that a faster compensation of non-periodic current comes at the price of "power fluctuation", and " torque ripple in the axis of the generator". As a result of this trade-off between fluctuation and speed, the technique required a decision making to be performed by engineers before setting up the compensator, which largely decreases its objectivity. Therefore, it is evident that the pq-theory based compensation is incapable of efficiently addressing the non-periodic load current compensation.

Compensation using Current's Physical Components theory

Another power theory utilized for the compensation of power quality degrading loads is proposed by Czarnecki, known as Current Physical Components (CPC) theory [50]. In this technique, the current waveform is decomposed into several components, each carrying a physical meaning, namely, active current, reactive current, scattered current, generated current, and unbalance current. CPC theory has been used for the compensation of various power quality degrading situations, namely, non-linear load, unbalanced load, pulsed loads, and systems with non-sinusoidal and imbalance supply voltage[52].

In [41], the CPC theory is used for the compensation of loads with the non-periodic voltage of a finite energy. For the CPC theory to be able to decompose such a load into the orthogonal components (active current, reactive current, and scatter current), several optimistic assumptions are made, such as infinite window length of the calculation, and continuity and finite energy of the voltage signal. Also, the proposed technique minimizes the source current only by minimization of the reactive current and not considering other components of the current.

In another work, CPC theory is utilized to compensate the non-periodic current using a hybrid time and frequency domain based compensator[36]. In this work the current components are compensated using two compensators; one (a thyristor controlled susceptance) responsible for reactive current and imbalance current compensation, and another (active filter) responsible for harmonic current and the rest of the non-periodic current. Lumping all the harmonic and non-periodic part of the current into "residual component", however, degrades the meaning of Current Physical Components. In other words, the non-periodic part of the current does not carry a physical meaning and is not compensated by a compensator that is designed specifically for such current waveform. Moreover, the proposed technique is incapable of simultaneously compensating the sharp edges and the slow variation of the cur-

rent waveform. Also, this method is not evaluated using the existing power quality criteria, as they are incapable of describing the non-periodic load.

Shortcomings of the Existing Techniques

The existing techniques for the compensation of the non-periodic load demonstrate several shortcomings listed below:

1. Single calculation window:

   Non-periodic load current consists of numerous quasi-harmonic components, and inter-harmonic noise. Therefore, unlike the frequency components of a periodic quantity, it might not share a greatest common divisor frequency. Moreover, there exists a large difference between the frequency of load various components of current to be compensated. Therefore, choosing a single value for the calculation window, which takes into account such variety of frequency components, largely decreases the efficiency of the existing techniques. In other words, in order to compensate the non-periodic current solely, based on the existing power theories, requires a voltage source converter with an extremely large rating, and simultaneously extremely large bandwidth. Therefore, an efficient technique would be able to decompose the current waveform into different frequency bands with different time window lengths.

2. Energy storage requirement:

   Compensation of non-periodic current requires active current injection. The reason is that the frequency components of the non-periodic load are not all multiple integers of the fundamental frequency. Therefore, there will be excess or deficient of active power over one cycle of power frequency which should be provided using an energy storage. The existing technique, however, does not consider such constraint in their design. Therefore, they are not capable of optimizing the energy storage

size which is one of the most salient cost factors of the design of non-periodic load compensator.

3. Decomposed components without meaning:

   All of the existing techniques are the mere extension of the techniques assuming periodic quantities. Therefore, the decomposed current components lose their meaning migrating from periodic quantities to non-periodic ones. An efficient technique for the compensation of non-periodic current would take into account the differences between periodic and non-periodic quantities while using the same framework used for the compensation of periodic quantities. Therefore, such technique has to decompose the current into components that are meaningful parts of the non-periodic current. As a result, it is possible to develop devices which are specifically designed to compensate each part of such current.

4. Absence of power quality indexes:

   None of the proposed techniques are evaluated using power quality indexes. The main reason is that most of the power quality indexes are explicitly defined based on the assumption of the periodicity of power quantities. An acceptable power quality index takes into account the difference between non-periodic and periodic quantity but is capable of describing the characteristics of both systems.

1.6 Contribution of this Dissertation

The method proposed in this dissertation is a hybrid time-frequency method to provide current reference for a co-located arrangement which is temporally distributed. This compensation technique consists of three parts, namely fast compensator, slow compensator, and reactive compensator. The first (fast compensator) and second (slow compensator) are time-domain based approaches and the third (reactive component compensator) is a frequency based method. The proposed technique is capable of compensating non-periodic loads in networks with distorted voltage sup-

ply, capable of compensating the unbalanced loads and poly-phase loads. Moreover, the design limitation of the proposed method, such as the active filter energy storage requirement, is discussed thoroughly. The proposed technique is validated using MATLAB simulation in conjunction with real-world data acquired from a steel mill cyclo-converter. Moreover, a real-time controller in the loop structure is utilized to verify the method using steel mill data. It should be noted that compared to the existing techniques of compensation of non-periodic loads, the proposed technique utilized faster and more sophisticated signal processing tools.

Moreover, three power quality indexes are proposed to develop supervisory control for the compensators and also evaluate the proposed technique. Three signal processing driven criteria, namely, modulation index, time-frequency distortion, and high frequency distortion index, are proposed to comply with the non-stationary behavior of the non-periodic load. Existing power quality criteria, such as Power Factor (PF) and Total Harmonic Distortion (THD) are incapable of describing the characteristics of non-periodic loads. The proposed approach demonstrates high capability in improving these power quality indexes.

This dissertation is organized as follows: Chapter 2 and Chapter 3 describe the development toward the proposed technique, Chapter 4 demonstrates the simulation and real-time results of this technique, Chapter 5 describes the practical considerations of building this technique, and Chapter 6 discusses the possible future works based on the development presented. Moreover, this dissertation is followed by four appendices that clarify different mathematical aspects of this work.

Chapter 2

Non-periodic Current Properties and Power Quality Indexes

A general frequency spectrum of a periodic and a non-periodic load are depicted in fig. 2.1. Loads with non-periodic current share two characteristics representable in the frequency domain [36]. First, instead of sharp spikes around the harmonic frequencies, the non-periodic current has rather a narrow band of frequencies around each harmonic, which is referred to as a "quasi-harmonic band". This part of the current results in a variation of the current waveform peak based on an envelope. This phenomenon could be modeled as an amplitude modulation of the component by a time-varying carrier. Any device for the compensation of this part of the current waveform requires a large window length (integer multiple of the fundamental frequency cycle) to be able to catch and filter the low frequency components of the signal. In the next chapter a high rating low bandwidth compensator is proposed for the compensation of such quasi-harmonic band of the spectrum.

The second frequency domain feature of non-periodic components is the presence of non-negligible frequency content between different harmonics, which is called "inter-harmonics noise" [36, 53]. These components could be amplified drastically if a traditional resonance based passive filter is used to compensate them. Therefore, extraction of a compensator control reference targeted toward this feature of the non-periodic components should have small window length (fraction of the fundamental frequency cycle), to be able to catch the high frequency components of the current

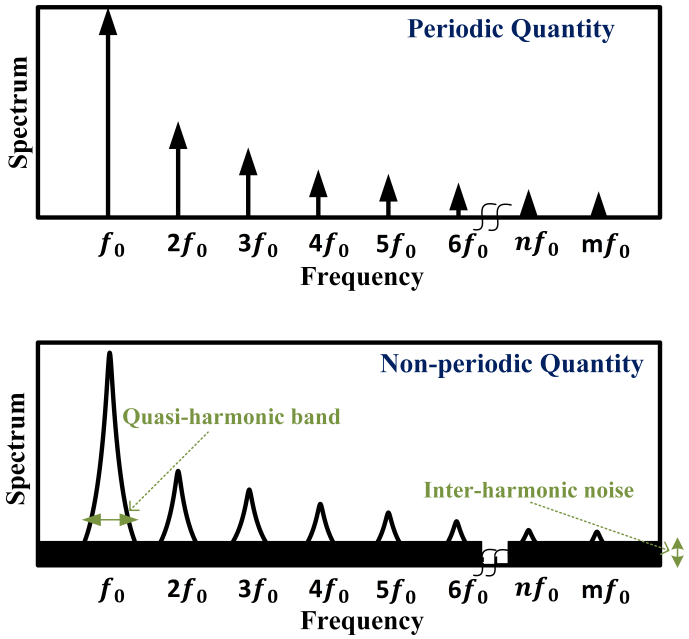

Figure 2.1: Frequency domain difference between the non-periodic and periodic quantities.

waveform. In the next chapter, a compensator named fast compensator is proposed for such purpose.

There is also a need for the elimination of reactive part of the current waveform, which is common between most of the power quality degrading loads. The window length required for the calculation of the reactive part of the current is equal to the fundamental frequency cycle.

As demonstrated in fig. 2.1, since the spectrum of the non-periodic current contains frequencies other than the power system frequency (e.g. 60 Hz) and their multiples, the well-known total harmonic distortion would result in an inaccurate representation of the harmonic distortion level. Moreover, the non-periodic current is non-stationary, which means its frequency spectrum demonstrates temporal variation. Therefore, it cannot be quantified using frequency-domain based power quality indexes. To alleviate these issues, three power quality indexes, capable of describing non-periodic loads are proposed.

2.1 Time-Frequency Distortion Index ($TFDI$)

In this work, a time-frequency based index is proposed to demonstrate the level of current distortion. Time-frequency domain analysis takes into account the time and frequency domain simultaneously [54]. Time-frequency based criteria has been recently utilized to define the active/ reactive part of the power (current) waveform [55]. In this work, the time-frequency analysis is used to describe the non-fundamental part of the current waveform. Similar to THD, $TFDI$ emphasizes the total power of the waveform excluding the power in the fundamental frequency of the current. In this work, Wigner-Ville time-frequency distribution (WVD) of the current waveform is used for the definition of the $TFDI$. The WVD distribution, $WVD_s(t,\omega)$, of the current waveform, $s(t)$, is calculated using the following equation:

$$WVD_s(t,\omega) = \frac{1}{4\pi^2}\iiint_{-\infty}^{\infty} IAC_s(u,\tau)\phi(\theta,\tau) \times e^{-j\theta t - j\tau\omega + j\tau u} d\theta d\tau du \quad (2.1)$$

where $\phi(\theta,\tau)$ is a two dimensional function,$\phi(\theta,\tau)$, (in Doppler-lag domain), called *kernel*. It is equal to "1" for the WVD. t and ω are time and frequency, respectively, and IAC_s is the *instantaneous auto-correlation* of the signal $s(t)$ defined as:

$$IAC_s(t,\tau) = s^*(t-\tau/2)s(t+\tau/2) \quad (2.2)$$

The WVD could be used to extract the frequency and time localization of the current waveform, which are necessary to define a criterion for non-periodic currents. This capability comes from the fact that WVD meets two requirements, namely, time marginal (TM), and frequency marginal (FM). These requirements are described as follows:

$$TM : \int_{-\infty}^{\infty} WVDs(t,\omega)d\omega = |s(t)|^2 \tag{2.3}$$

$$FM : \int_{-\infty}^{\infty} WVDs(t,\omega)dt = |S(\omega)|^2 \tag{2.4}$$

The signal energy (E_S) over the window of calculation (T) is calculated using the following equation:

$$E_s = \frac{1}{T}\int_0^{\omega_{max}} \int_0^T WVD_i(t,\omega)dtd\omega \tag{2.5}$$

where ω_{max} is the largest frequency components of the signal which is based on the Nyquist–Shannon theorem equal to half of the sampling frequency.

The energy of the fundamental harmonic, E_{s1}, (which is responsible for the actual transfer of power from the source to the load) is calculated using the following equation.

$$E_{s1} = \frac{1}{T}\int_{\omega_0-\varepsilon}^{\omega_0+\varepsilon} \int_0^T WVD_i(t,\omega)dtd\omega \tag{2.6}$$

where ε is considered a few frequency bins in the neighborhood of the fundamental frequency.

Finally, the time-frequency distortion index is defined as:

$$TFDI_s = \sqrt{\frac{E_s - E_{s1}}{E_{s1}}}\% \tag{2.7}$$

Note that, for periodic quantities, this definition coincides with the traditional definition of total harmonic distortion calculated using Fourier transform (Eq. 2.8). On the other hand, THD loses its efficiency for calculating the harmonics distortion of the non-periodic (non-stationary) signal.

$$THD_s = \sqrt{\frac{\sum_{n=0}^{\infty} \quad I(n\omega_0)^2 - I(\omega_0)^2}{I(\omega_0)^2}}\% \tag{2.8}$$

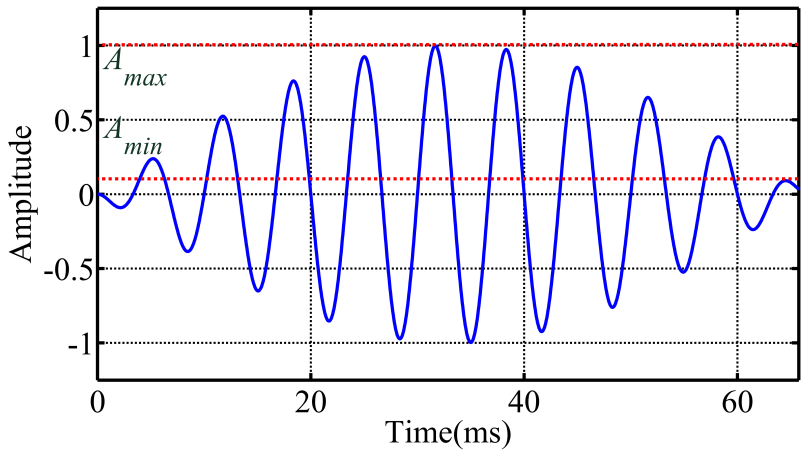

Figure 2.2: Demonstration of an amplitude-modulated waveform.

Please refer to Appendix A for the discussion about the equality of THD and $TFDI$ for periodic components.

2.2 Modulation Index (m_i)

As demonstrated in [36], one of two main characteristics of non-period currents, besides the existence of inter-harmonic noise, is the presence of some form of amplitude modulation which results in spreading the frequency content around each harmonic. In this work, modulation index, defined in (2.9), is utilized as a fast time-domain method to demonstrate the level of amplitude modulation, and therefore the degree of the non-periodicity of the current. Assume that the current waveform of a non-periodic current is depicted fig. 2.2. The modulation index, m_i, for such a case is calculated as:

$$m_i(t) = \frac{A_{max} - A_{min}}{A_{max} + A_{min}} \tag{2.9}$$

where A_{max} and A_{min} are the maximum value of the modulated signal envelope, respectively.

One of the main advantages of modulation index criterion, compared to the frequency based criteria is the fact that its calculation merely needs half of one period of

the modulation frequency. On the other hand, to calculate the frequency based criteria, such as distortion factor [40], at least on the period of the modulation frequency is needed.

2.3 High Frequency Distortion Index ($HFDI$)

The existing criteria, $TFDI$ and m_i are appropriate to access the overall performance of a compensator for non-periodic currents. For the purposes of evaluating the performance of compensation within a particular frequency range another metric is developed. This is important since compensation may be done is frequency intervals depending on the power ratings and bandwidth limitations of particular equipment. Thus, a targeted index, typically in the high frequency where compensation is more limited is useful. For such purpose, High Frequency Distortion Index ($HDFI$) is proposed. Similar to the $TFDI$, $HDFI$ finds the ratio between the energy in the unwanted frequency components and the energy in the fundamental frequency. However, instead of calculating the energy over the whole the frequency range, $HDFI$ calculates the energy in components in a specified frequency interval above the fundamental. Therefore, the $HDFI$ is simply calculated using the following equations:

$$E_{HF} = \frac{1}{T}\int_{\omega_{SC}}^{\omega_{max}}\int_{0}^{T} WVD_i(t,\omega)dtd\omega \tag{2.10}$$

$$HFDI_s = \sqrt{\frac{E_{HF}}{E_{s1}}}\% \tag{2.11}$$

where E_{HF} is the energy in the high-frequency range of the signal and ω_{SC} is the bandwidth of the slow compensator (which will be discussed in Section 3.3).

Chapter 3

Proposed Compensator Control References

The method proposed in this dissertation for the compensation of non-periodic load provides control references for three co-located devices, each corresponding to one moving calculation window and one decomposed part of the compensated current. These compensators are slow compensator with high power rating, large calculation window, and low switching frequency; fast compensator with lower power rating, shorter calculation window, and higher switching frequency; and the reactive compensator which is an ordinary static VAR compensator (SVC). In this chapter, the structure of this proposed control reference is discussed. Moreover, a new structure is proposed to share the bandwidth and rating between the compensators.

The complete structure of the compensator with these three compensation devices are shown in fig. 3.2. Each one of the proposed devices has a particular moving window for the calculation of their current reference. The fast compensator window length is a short fraction of the generated voltage frequency period which results in higher compensation speed compared to other non-periodic compensation techniques, which use windows equal or larger than the fundamental frequency period of the generated voltage. For example, in [48], a window length equal to ten times the period of the fundamental frequency of the voltage is chosen. The reactive compensator window length is one cycle of generated voltage frequency period. The window length of the slow compensator is larger than the other two compensators since it is in charge of the low-frequency part of the non-periodic current. Therefore, to ideally achieve zero non-periodicity, the slow compensator must realize infinite window length

[42]. However, since such design is not realizable, the proposed algorithm uses an adaptive fuzzy algorithm to look for optimized window length. The optimized window is found in a way that the power quality requirements are met while having the minimum energy storage size for the slow compensator. The tri-window structure of the proposed method is shown in fig. 3.1.

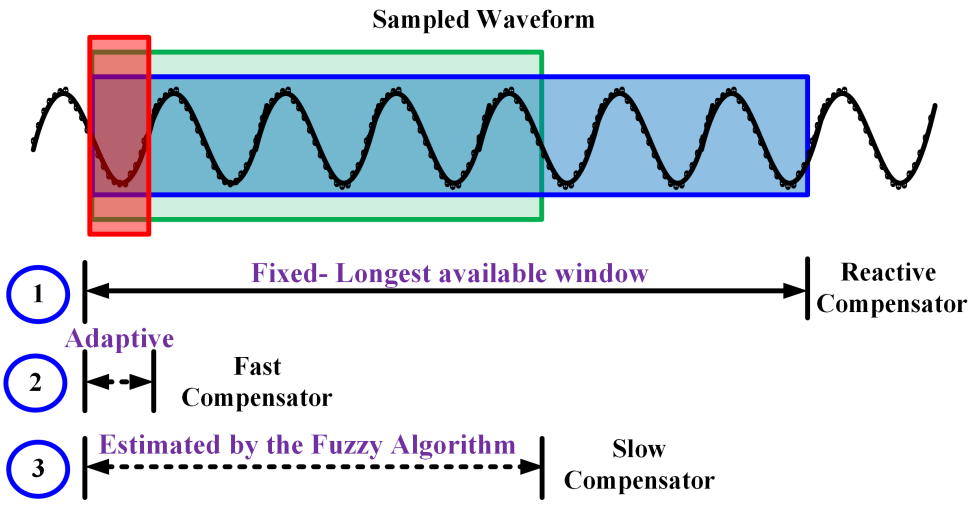

Figure 3.1: The tri-window structure of the proposed method.

3.1 Reactive Compensator

In order to eliminate the reactive current, a Static VAR Compensator is used. The reference current for this compensator is calculated using the following equations:

$$q(t) = v(t - \frac{T_0}{4})(i(t) - i_{FC}(t)) \tag{3.1}$$

$$Q(t) = \frac{1}{T_0}\int_t^{t+T_0} q(\tau)d\tau \tag{3.2}$$

$$B_e = \frac{Q}{{V_1}^2} \tag{3.3}$$

$$i_{R_1}(t) = B_e v(t - \frac{T_0}{4}) \tag{3.4}$$

$$i_{Rem_{RC}} = i_L - i_R \tag{3.5}$$

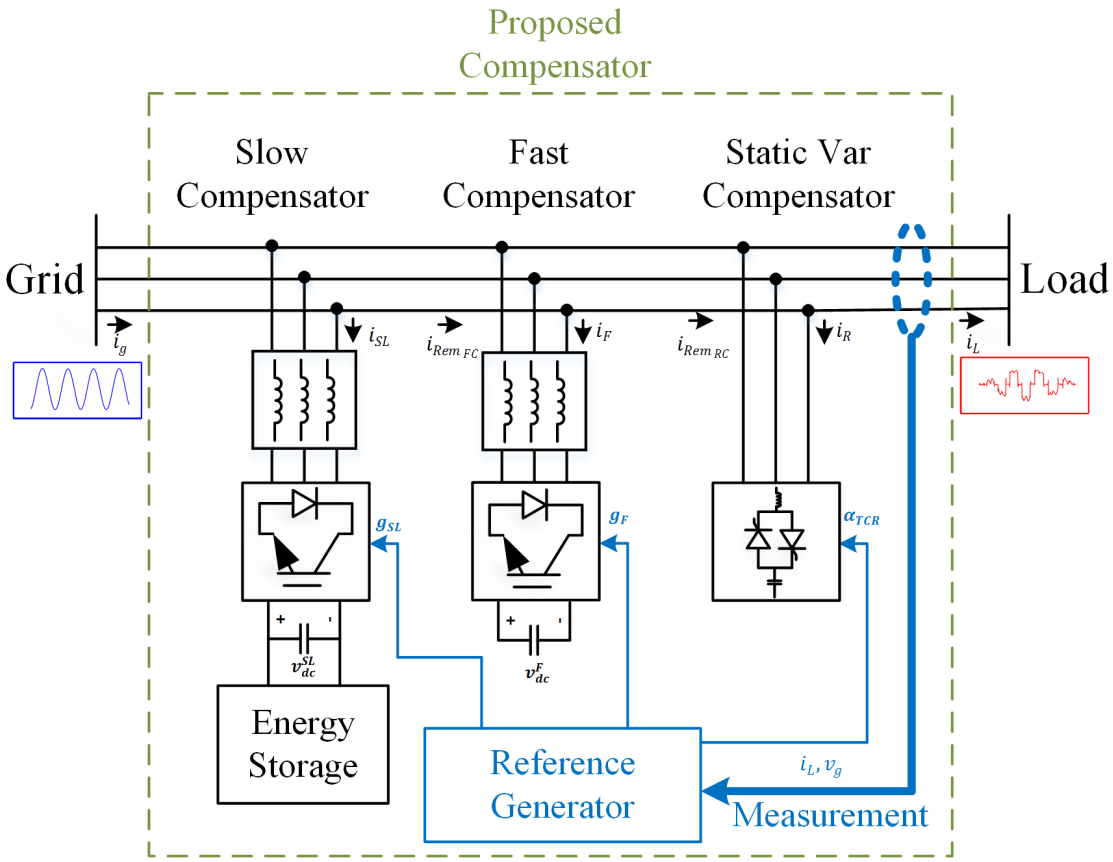

Figure 3.2: Structure of the proposed compensator.

where q is called instantaneous reactive power, Q is reactive power of the load, T_0 is the period of one cycle of power frequency, B_e is the equivalent susceptance, V_1 is the RMS value of the fundamental voltage, i_R is the reactive current reference,and $i_{Rem_{RC}}$ is the remaining current after the reactive compensation that will be loaded to the fast compensator.

3.2 Fast Compensator

Passive filters prove ineffective in the compensation of loads with non-periodic current since the inter-harmonic noise would coincide with their resonant frequencies. Therefore, active filters are required to filter out the high-frequency and low-frequency part of the current waveform. A novel adaptive fast compensator (FC) control refer-

ence is proposed in this dissertation for the compensation of high-frequency content of the current. The main purpose of this compensator is to make sure that the compensator with the large rating (slow compensator) does not require high bandwidth. Therefore, this compensator is responsible for conditioning the current waveform to a bandwidth level that is manageable by the slow compensator.

The reference current of the fast compensator is calculated using the following set of equations:

$$p_{FC}(t) = v(t) i_{Rem_{RC}}(t) \tag{3.6}$$

$$P_{FC}(t) = \frac{1}{kT_0} \int_t^{t+kT_0} p_{FC}(\tau) d\tau \tag{3.7}$$

$${V_{FC}}^2(t) = \frac{1}{kT_0} \int_t^{t+kT_0} v(\tau)^2 d\tau \tag{3.8}$$

$$G_{e_{FC}}(t) = \frac{P_{FC}(t)}{{V_{FC}}^2(t)} \tag{3.9}$$

$$i_{FC}(t) = i_{Rem_{RC}}(t) - G_{e_{FC}} v(t) \tag{3.10}$$

$$i_{Rem_{FC}}(t) = i_{Rem_{FC}}(t) - i_{FC}(t) \tag{3.11}$$

where p_{FC} is instantaneous power of the load after reactive compensation, P_{FC} is the power average over a window length which is equal to the fraction of supply voltage period (kT_0), ${V_{FC}}^2$ is the voltage RMS calculated over the same window length (kT_0), $G_{e_{FC}}$ is the equivalent conductance of the load after reactive compensation over the same window length (kT_0), i_{FC} is the reference current of the fast compensator, and $i_{Rem_{FC}}$ is the remaining current after the fast compensation.

The final purpose of any compensation is to achieve a constant equivalent conductance. However, such goal requires an active filter with very high rating, large energy storage, and large bandwidth. In this dissertation, the purpose of the fast compensator is to compensate the low power-high frequency part of the current waveform. This goal is achieved through adaptively controlling the fast compensator window length (kT_0).

In general the load equivalent conductance seen by the fast compensator could be written as follows:

$$G_{e_{FC}}(t) = \frac{\overline{P} + \widetilde{p}_{LF}(t) + \widetilde{p}_{HF}(t)}{\overline{V^2} + \widetilde{v^2}_{LF}(t) + \widetilde{v^2}_{HF}(t)} \tag{3.12}$$

where symbols "$\widetilde{}$" and "$\bar{}$" demonstrate time-varying and constant quantities, respectively, and subscript "LF" and "HF" demonstrate low frequency and high frequency components, respectively.

The constant equivalent conductance is achievable when both nominator and denominator have zero time-varying components. For such purpose, two moving average FIR (finite impulse response) filters (equations (3.8) and (3.9)) are used in Fryze power theory. However, the basic Fryze power theory based compensator ($k = 1$) does not allow for adaptive sharing of the bandwidth between compensators and also compensation of non-periodic current.

3.3 Slow Compensator

The non-periodic part of the current has theoretically infinity large period [42]. Therefore, the higher compensation window results in smoother compensation and higher power quality. The existing attitude for non-periodic compensation in the literature is that, the longer the window size, the better the compensation quality. Though it is correct in general, the longer window also implies longer transient response. Therefore, by choosing possibly a smaller window (with similar power quality of longer windows) the transient time after a load change could be minimized without compromising the power quality. Moreover, by decreasing the window length size, the required bandwidth of the slow compensator is decreased.

Therefore, in order to remove the non-periodic and low frequency part of the current, an active filter, whose window length is adaptively modified is designed. The window length is chosen so that it has the minimum size to achieve acceptable

modulation index. The slow compensator current is calculated using the following relations:

$$p(t) = v(t) i_{Rem_{FC}}(t) \tag{3.13}$$

$$P(t) = \frac{1}{T} \int_{t}^{t+T} p(\tau) d\tau \tag{3.14}$$

$$G_{e1} = \frac{P}{{V_1}^2} \tag{3.15}$$

$$i_{SC}(t) = i_{Rem_{FC}}(t) - G_{e1}(t) v_1(t) \tag{3.16}$$

where G_{e1} is the *total power equivalent conductance of the fundamental frequency* which reflects the equivalent conductance of the load in case all the current is being transferred with the fundamental frequency, i_{SC} is the current being compensated by the slow compensator, and T is the window length for the calculation of equivalent conductance.

The ultimate goal of the slow compensator is to achieve the equivalent conductance with zero oscillation. However, in the practical case, such goal is not achievable since it requires an infinitely large energy storage. In this work, a fuzzy-based algorithm is proposed to minimize the oscillating part of the equivalent conductance by adaptively modifying the length of the calculation window:

$$G_e(t) = G_{e1}(t) + \widetilde{G}_e(t) \tag{3.17}$$

where $G_e(t)$ is the measured load equivalent conductance and $\widetilde{G}_e$ is the oscillating part of the equivalent conductance. The goal of the slow compensator is to achieve constant G_{e1}, and therefore zero $\widetilde{G}_e(t)$.

It could be proven that for a non-periodic current, the oscillating part of the equivalent conductance is proportional to several factors as follows.

$$\widetilde{G}_e \quad \propto \quad \frac{sin(2\pi lq)}{l} \tag{3.18}$$

$$for \quad l = \frac{T}{T_0} \tag{3.19}$$

$$for \quad q = \pm mk \tag{3.20}$$

where n is the order of existing harmonics in the current (odd numbers for power systems), m is the order of existing harmonics in the modulating signals (odd numbers for regular modulating signals), k is the modulation ratio ($\frac{\Delta\omega}{\omega_0}$), $\Delta\omega(= 2\pi f_m)$ is the modulation frequency, and ω_0 is the power system frequency. Please see the Appendix B for detailed mathematical explanation.

It could be concluded that in order to reach zero oscillating conductance (pure sinusoid current), one of two requirements shall be met; (1) infinite window length ($1/T = 0$), and (2) integer $2lq$ ($cos(2\pi lq) = 0$) . Though the former is unrealizable (infinite energy storage is needed), the latter could be realized using a minimization algorithm in a way that the window length (l) is to be manipulated to reach a minimized error signal $e(n, m, l)$:

$$e(n, m, l) = 2lq - round(2lq), for\ n = 3, 5, ..,\ m = 1, 3, ... \tag{3.21}$$

However, it is not feasible to minimize all the errors with one particular window (l). Therefore, an algorithm is needed that incorporates the importance of each current harmonics and modulation harmonic (n, m) in finding the best window size.

The flowchart of the proposed Mamdani-based fuzzy algorithm part of the slow compensator is shown in fig. 3.3. The method uses FFT calculation of the remainder current ($i_{rem} = i_L - i_F - i_R$) to find the dominant harmonics, the modulation frequency ($\Delta\omega$), and modulation ratio (k). Using FFT for such purpose results in less computational burden compared to other methods such as Kalman filtering used in [56] for the similar purpose. The fuzzy logic uses the modulation index reference (in

this work it is set $m_i = 5.3\%$ for acceptable fluctuation) to define different regions of the fuzzy logic. For each window length three decisions are possible, namely, *accepted window*, *good window*, and *rejected window*. The optimized window is selected in the following way:

- find the decision of the algorithm for window length $l = 1$ to l_{max}.
- if there exists several window length (l) with $ACCEPTED$ response, choose the smallest one.
- if there is no $ACCEPTED$ response, choose the largest $GOOD$ window length.
- if there is no $ACCEPTED$ or $GOOD$ window, choose the maximum window length (l_{max}).

The fuzzy logic assures that while we meet the power quality criteria, maximize the slow compensator utilization (and therefore load sharing), minimize the transient response of the compensator, and also minimize the overall implementation cost.

3.4 Sharing between Fast- and Slow Compensator

3.4.1 Sharing of Bandwidth

As previously mentioned, the fast compensator function is to condition the current waveform, to a level that is manageable by the slow compensator. In other words, in the design phase, the bandwidth of the fast compensator is being determined by the available bandwidth of the slow compensator. Moreover, the fast compensator power rating is by definition a fraction of the slow compensator power.

In this dissertation, to realize the sharing of bandwidth between the compensators, the window length of the fast compensator is set to a fraction of one cycle of power frequency (k). Figure 3.4 shows the frequency response of the moving average

integrator for different window lengths (k). It is apparent that larger window size of the fast compensator results in more substantial high-frequency removal. Therefore, by defining the k factor in the design phase, the bandwidth and power of the load could be easily shared between the two compensators. It is noted that other FIR filters could also be utilized for the purpose of low pass filtering. However, as it will be shown in Section 4.4.3, in this work the moving average low pass filter is used, since it allows using the recursive integrals which largely decreases the computational burden on the processor.

Figure 3.5 demonstrates the $3dB$ bandwidth of the line current after the fast compensation for different window lengths. This figure could be used for designing the sharing scheme of the bandwidth between fast- and slow compensators. As an example, if the available (required) bandwidth of the slow compensator is $1.4kHz$, the fast compensator window length is set to $30°(k = 0.083)$ suffices.

3.4.2 Sharing of Rating

The fast compensator is a power conditioner before the main (slow) compensator. Therefore, its power rating should be, by definition, a fraction of the slow compensator power rating. In this work, the ratio of the fast compensator to the rating of the slow compensator is predetermined in the design phase and is equal to *Ratio* parameter.

3.5 Summary

This chapter is developing a novel tri-window based compensator for the compensation of loads with the non-periodic current. This compensator consists of three co-located devices with different calculation window, called fast compensator, reactive compensator, and slow compensator. One of the challenges with the proposed method is that, though the reactive compensator current and slow compensator cur-

rents are mathematically orthogonal, the fast compensator current is not orthogonal to them. However, since these components are sequentially ordered, the orthogonality requirement is waived.

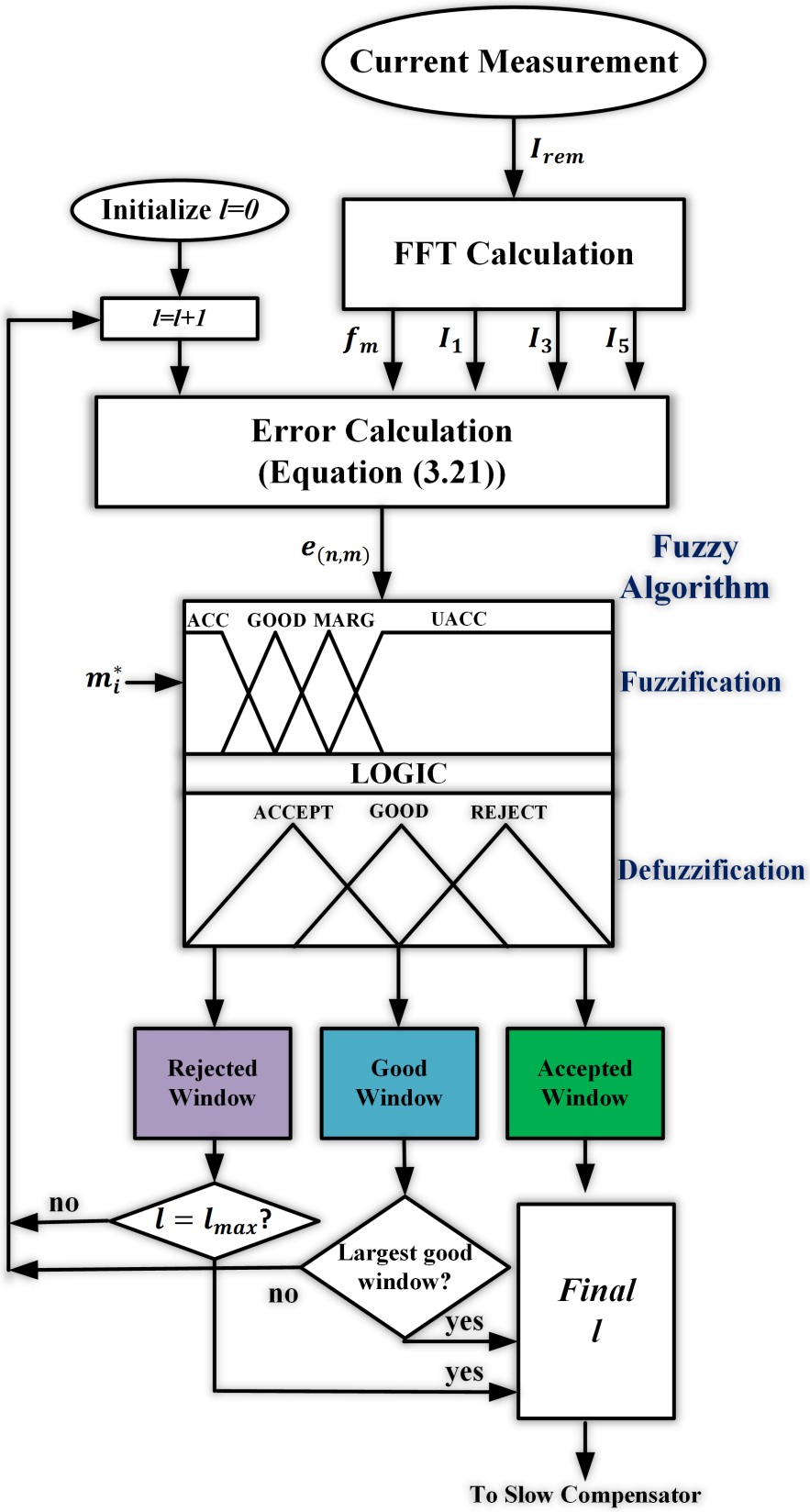

Figure 3.3: Flowchart of the adaptive fuzzy algorithm for modification of slow compensator window length.

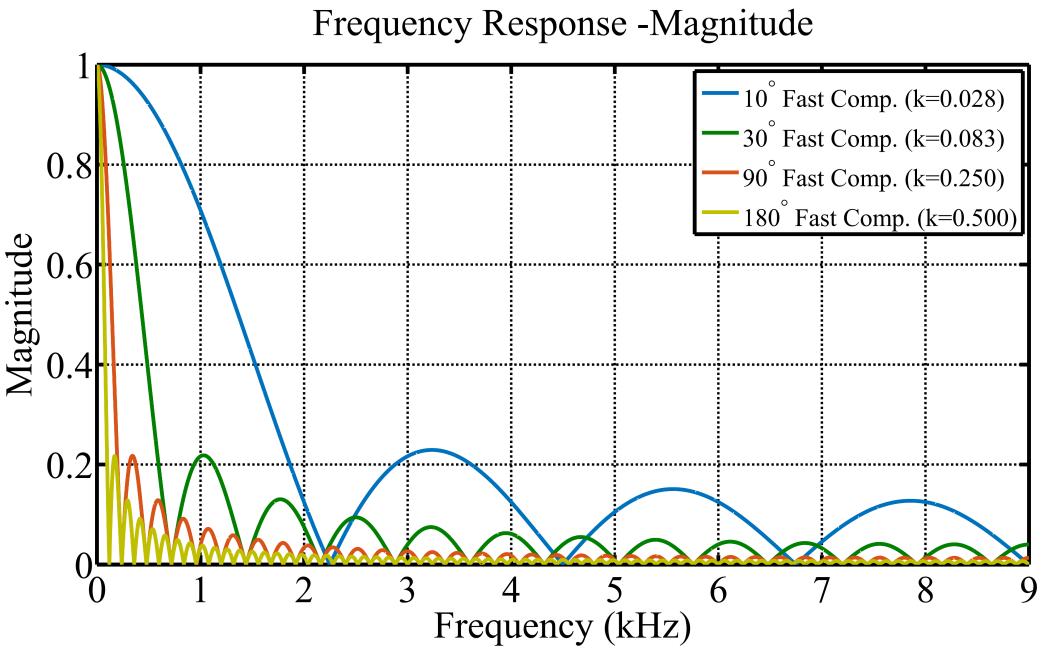

Figure 3.4: Frequency response of the moving average integrator for different window lengths.

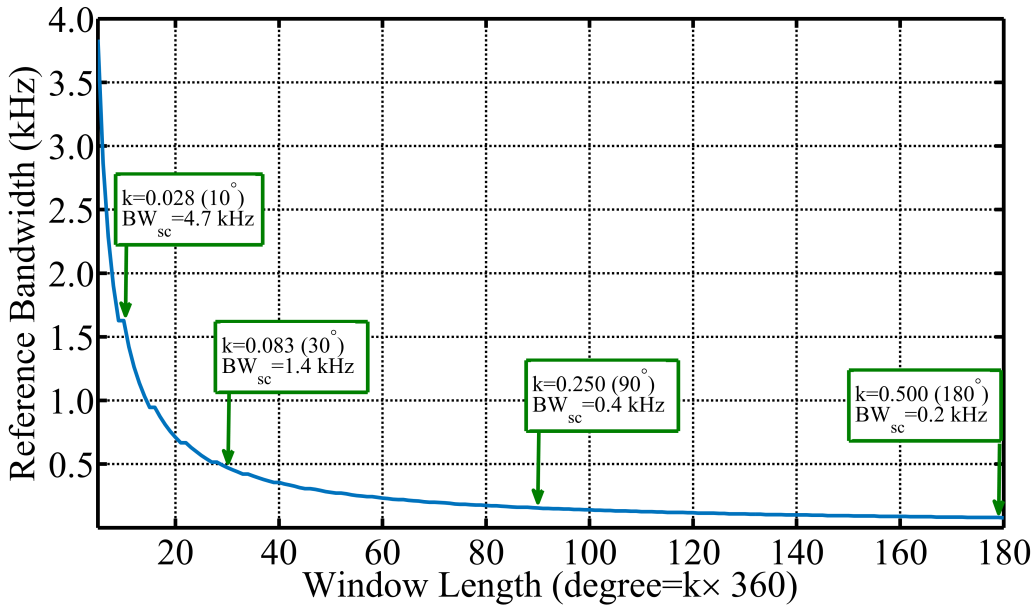

Figure 3.5: The bandwidth of the current waveform after the fast compensation with different window lengths.

Chapter 4

Simulation and Real-time Verification

4.1 System Under Study

To verify the proposed tri-window algorithm, real-world data acquisition was performed on a running steel mill with six units of six-pulse cyclo-converter bridge, each supplying a 7.7 MW synchronous motor. The detailed circuit diagram of the system under study is shown in fig. 4.1. Description and operating condition of four loading cases of the motor are shown in Table 4.1. It is noted that in this table f_{motor} demonstrates the motor rotation speed.Moreover, the current waveforms for these cases are demonstrated in the left column of Fig. 4.2. Results for each case assume an ideal tracking of the references generated using the method described in chapter 3. Thus, current tracking error in an actual implementation will result in reduced performance that depends on specific implementation issues such as conversion and computation delays and switching frequency limitations.

4.2 Simulation Result

In this section the results of the proposed algorithm is demonstrated using real-world data acquired from a local steel mill and processed using Matlab. A sample design specification is also used to demonstrate the technique efficiency. For such purposed the bandwidth reference (BW^*_{SC}) is set at $1.4kHz$ and the power rating ratio ($Ratio^*$) is set at 50% (0.5).

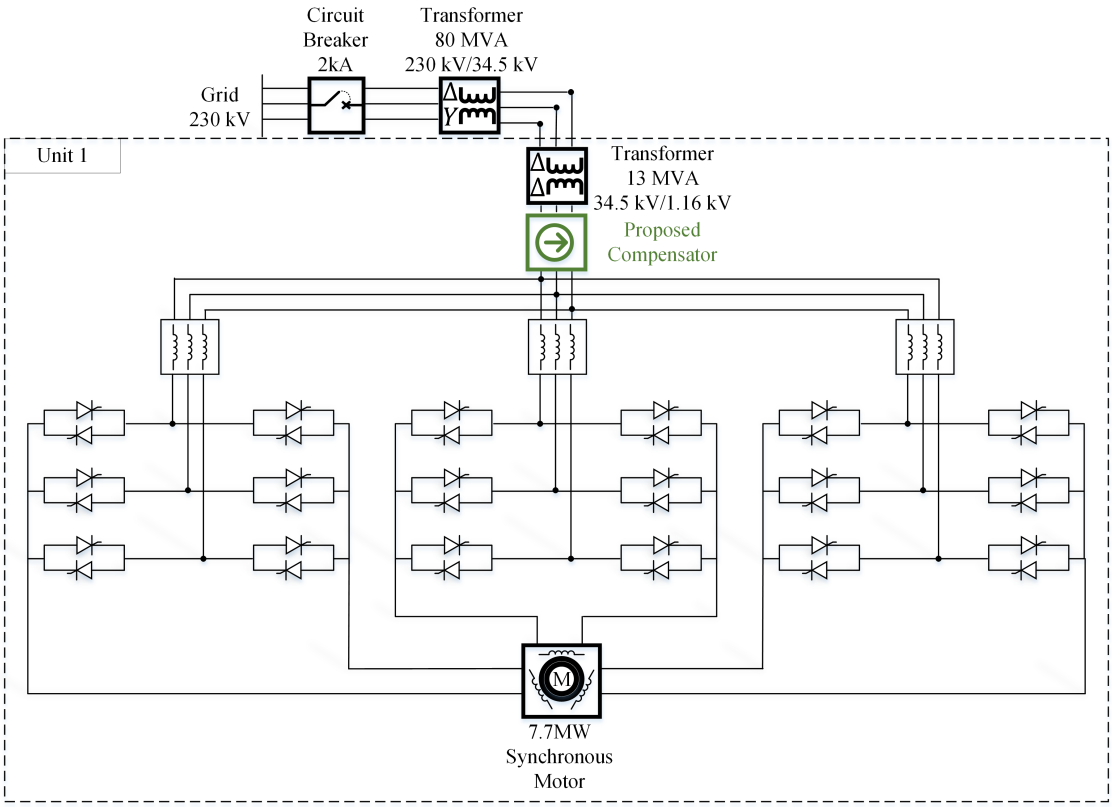

Figure 4.1: The circuit diagram of the steel mill cycloconverter.

4.2.1 Fast Compensator

The main function of the fast compensator is to filter out the high-frequency content of the current in a way that the slow compensator, which has a higher power rating active filter, does not require high switching frequency devices. Fig. 4.3.(d) demonstrates the current waveform of the fast compensator for $Ratio^*$ equal to 0.5. Fig. 4.3.(f) and (g) also demonstrate the difference between the line current after the compensation with and without using the adaptive scheme for the fast compensation, respectively. Though the final result without the adaptive scheme has higher power quality, it might not be practically achievable as the power rating of the fast compensator, in this case, is about 73% of the slow compensator.

The specification of the fast compensator for loading of $case1$ (for data acquisition by sampling rate of $37.3kHz$) are: $SCALE = 0.68$ (power sharing scale), $k = 0.083$

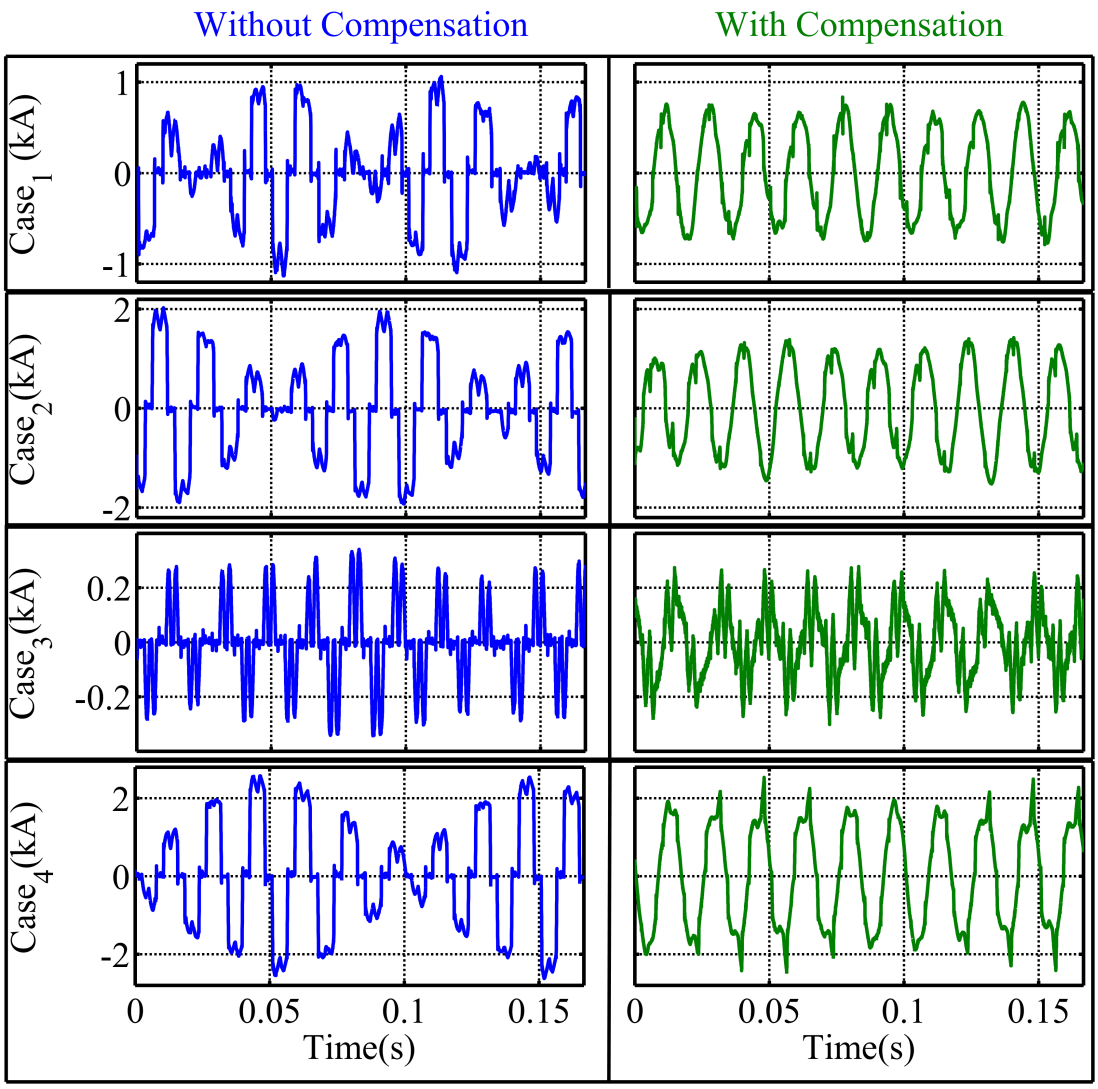

Figure 4.2: Current waveform for four loading cases of the cyclo-converter and their corresponding current after the compensation

(window length) $BW_{FC} = 9kHz$ (bandwidth), $P_{rating_{FC}} = 209.7\ kVA$ (rating power).

4.2.2 Slow Compensator

The slow compensator is the main part of the tri-window compensator whose role is the compensation of the non-periodicity in the load current. Fig. 4.3 demonstrates different aspects of the slow compensation for the loading *case* 1. Fig. 4.4a depicts the modulation index value for different window lengths of the slow compensator. It

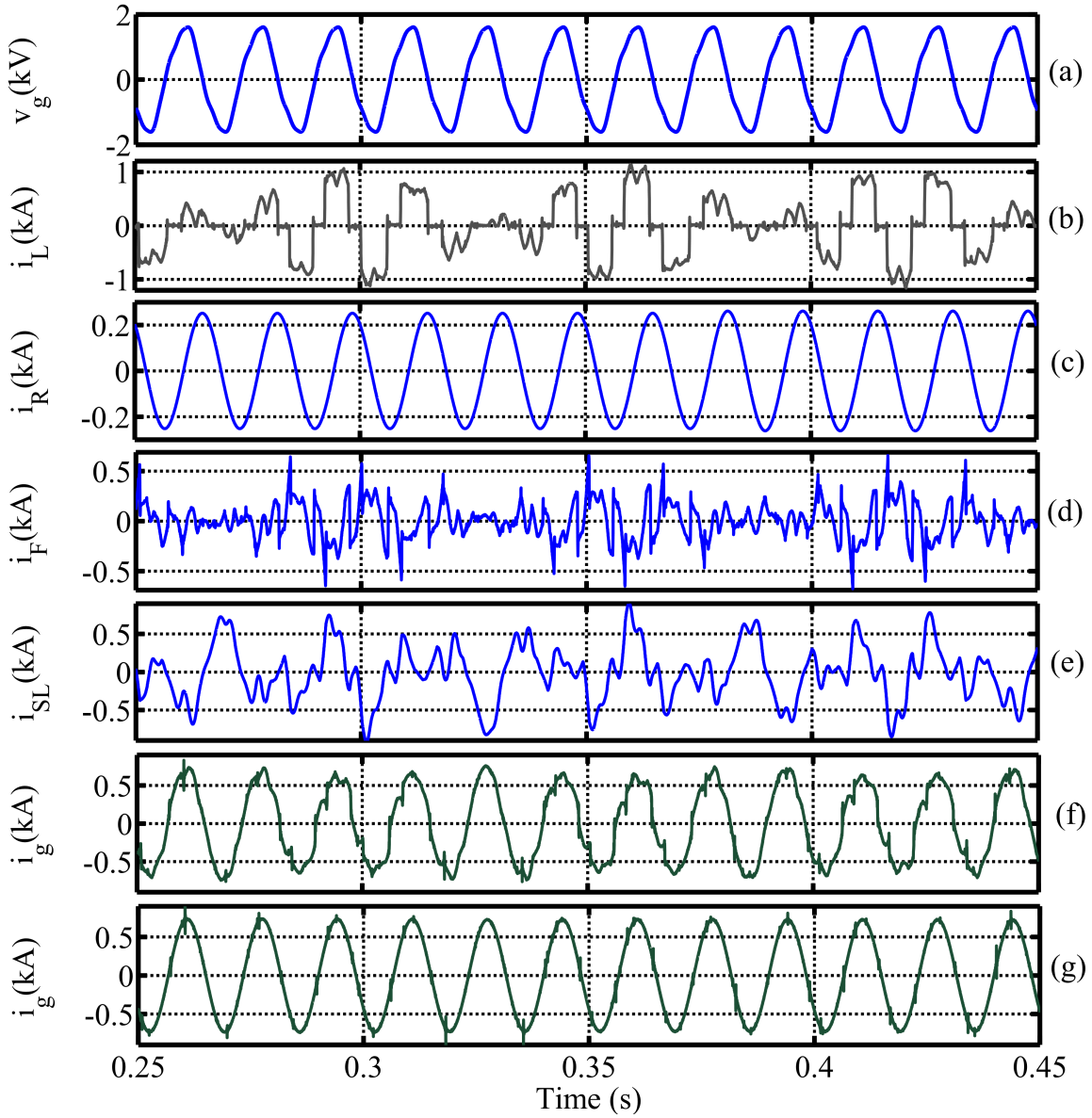

Figure 4.3: Voltage and current waveform of the compensator :(a) line voltage, (b) load current waveform acquired from measurement data (c) reactive compensator current, (d) fast compensator current ($Ratio^* = 0.50$), (e) slow compensator current, (f) line current after compensation (with $Ratio^* = 0.5$), (g) line current after compensation (with full scale fast compensator)

is evident from the figure that with the increase of the window length, generally, the modulation index decreases. However, there are some local minima, estimated by the slow compensator fuzzy logic, which result in modulation indexes comparable to that of larger windows, e.g. $T = 11T_0$ for loading *case* 1.

The line current waveforms for different window length are presented in fig. 4.4b . It could be concluded from the zoomed-in figure that the line current waveform after slow compensation with $T = 11\ T_0$ and $T = 22\ T_0$ have the lowest amplitude modulation.

Moreover, Fig. 4.3.(e) demonstrates the slow compensator waveform for the compensation of the non-periodicity of the current. The specification of the slow compensator for loading of $case1$ (for data acquisition by sampling rate of $37.3kHz$) are: $l = 11$ (window length), $BW^*_{SC} = 1.4\ kHz$ (bandwidth), and $P_{rating_{SC}} = 421.0\ kVA$.

Fuzzy Algorithm

The result of the fuzzy logic based adaptive window estimator of the slow compensator for loading *case* 1 is shown in fig. 4.3c. It is shown that for this case, two windows have acceptable results, namely, $T = 11T_0$ and $T = 22T_0$. Therefore, the window with a smaller size ($T = 11T_0$) is chosen by the slow fuzzy logic as the optimum window. The result of the estimated window by the fuzzy logic is completely in line with the calculated results from fig.4.4a.

Energy Storage

An energy storage system is required to keep the dc-link voltage of the slow compensator constant, which without the use of the proposed fuzzy algorithm, occurs only if the dc-bus storage is gigantic. The compensator's energy storage should store the energy difference between the maximum output power and minimum output power. This value depends on the chosen window length of the compensator. The energy storage capability against the chosen time window is formulated as follows:

$$\Delta E = \int_0^T v(t) i_C(t) dt \tag{4.1}$$

As demonstrated in fig. 4.3d, the energy storage size increases with the increase in the compensator window length. Using the fuzzy logic adaptive window estimator,

a window length $T = 11T_0$ is chosen which demonstrates the same power quality as of a design with $T = 22T_0$, while its energy storage requirement is about 2/3 of the energy storage of its counterpart. It is also evident, that only by increasing the window length the power quality is not necessarily improved since the modulation index of a design with $T = 11T_0$ is much smaller than that of $T = 24T_0$.

Table 4.1: Load description and power quality indices before and after the compensation.

Number	Description	Before Compensation	Compensation Parameters	After Compensation
Case 1	$f_{motor} = 16.4Hz$	$m_i = 73.9\%$ $TFDI = 71.1\%$ $HFDI = 8.35\%$	$SCALE = 0.68$ $T = 11T_0(l = 11)$ $P_{Rating_{RC}} = 131.8kVAr$ $P_{Rating_{FC}} = 209.9kVA$ $P_{Rating_{SC}} = 421.0kVA$	$m_i = 7.3\%$ $TFDI = 19.1\%$ $HFDI = 1.3\%$
Case 2	$f_{motor} = 12.4Hz$	$m_i = 69.6\%$ $TFDI = 67.3\%$ $HFDI = 5.8\%$	$SCALE = 0.66$ $T = 24T_0(l = 24)$ $P_{Rating_{RC}} = 169.6kVAr$ $P_{Rating_{FC}} = 381.0kVA$ $P_{Rating_{SC}} = 755.6kVA$	$m_i = 10.9\%$ $TFDI = 18.5\%$ $HFDI = 1.4\%$
Case 3	$f_{motor} = 10.0Hz$	$m_i = 81.7\%$ $TFDI = 115.9\%$ $HFDI = 7.6\%$	$SCALE = 0.38$ $T = 13T_0(l = 13)$ $P_{Rating_{RC}} = 37.3kVAr$ $P_{Rating_{FC}} = 53.7kVA$ $P_{Rating_{SC}} = 108.8kVA$	$m_i = 4.0\%$ $TFDI = 77.8\%$ $HFDI = 5.0\%$
Case 4	$f_{motor} = 5.5Hz$	$m_i = 76.1\%$ $TFDI = 77.5\%$ $HFDI = 8.5\%$	$SCALE = 0.53$ $T = 6T_0(l = 6)$ $P_{Rating_{RC}} = 166.9kVAr$ $P_{Rating_{FC}} = 387.2kVA$ $P_{Rating_{SC}} = 821.6kVA$	$m_i = 2.5\%$ $TFDI = 35.5\%$ $HFDI = 3.8\%$

4.2.3 Reactive Compensator

The current waveform of the reactive compensator is shown in Fig. 4.3. (c).The rating of the reactive compensator for the compensation of *case* 1 load is $P_{rating_{FC}} = 131.8\ kVAr$. It should, however, be noted that the focus of this section is on the behavior of the fast and slow compensators. The reason is that the reactive compensator does not contribute to the proposed power quality indexes (m_i, $TFDI$, and

$HFDI$). The reason is that the reactive compensator merely shifts the current phase and modifies the magnitude of the fundamental component of the current to minimize the phase displacement between current and voltage waveforms.

4.3 Power Quality Criteria

In this section, the result of the proposed algorithm is evaluated using the introduced power quality criteria.

Time-Frequency Distortion Index

Table 4.1 demonstrates the $TFDI$, the overall quality measure of the compensator, before and after the compensation. It is evident that the $TFDI$ decreases, in all cases. The level of improvement of $TFDI$, however, depends on the level of existing inter-harmonic noise.

Modulation Index

Fig. 4.4a demonstrates the modulation index, the quality measure of the slow compensator, for different window length calculated for $case1$. As also predicted by fig. 4.3c, for window length $l = 11, 22$ the compensated current has the lowest modulation index. Moreover, Table 4.1 shows the modulation index for different loading of the cyclo-converter before and after the slow compensation. In all the cases, the m_i reaches the accepted region after the compensation.

High Frequency Distortion Index

Table 4.1 demonstrates the $HFDI$, the quality measure of the fast compensator, before and after the compensation. It is evident that the $HFDI$ decreases, in all cases. The level of improvement of $HFDI$, however, depends on the level of existing inter-harmonic noise in the responsibility bandwidth of the fast compensator.

4.4 Real-time (RT) Implementation of the Tri-window Compensator

After verification of the technique using real-world data, it is necessary to evaluate the technique in real-world condition. Therefore, a real-time test setup is designed to test and evaluate the proposed compensator. In this structure, the load current and voltage are simulated in real-time and are generated as an analog voltage output. Therefore, the tri-window compensator behaves as a controller-in-the-loop (CIL) and generates the reference current required for each compensator as output analog voltage.

4.4.1 Real-Time Test Setup

The schematic of the RT test setup for the evaluation of the proposed technique is shown in Fig.4.4. This setup consists of two RT controllers and three I/O connectors.

In this design, the first controller, a *PXI 8176*, is booted up into RT operating system (RTOS) and emulates the load based on the model proposed in Appendix D. The data of this model is loaded on the RT machine hardware, and a LabVIEW RT graphical code generates the line voltage and the load current waveforms onto the analog output. The analog output card on this board (*NI 6713*) has a large enough buffer size (16354 samples) to emulate the load with the high sampling frequency. It is noted that the RTOS assures that the real-time operation of the algorithm is performed within the maximum calculation window.

The second controller is used to calculate the current reference and output the waveforms onto the line emulator. For this purpose, a *National Instrument PXI 8108 controller* is used which is a *Core 2 Duo 2.53 GHz* RT embedded controller with 80 *GB* hard drive. This controller is also booted into an RTOS. It acquires the data using high speed *NI-PXI-6143* data acquisition card (*250Ksample/s*) and generates

the waveform onto another high-speed data acquisition card (*NI-PXI-6221* with *833 kSample/s*). The current reference of the compensators is calculated using C code and was loaded to the RT machine using LabWindows/CVI RT module. A minimal example of this code could be found in Appendix 4.4.3.

The line emulator consists of two simple I/O connectors (*NI SCB-68*) that facilitate the connection between the load emulator and the compensator emulator. And finally, the oscilloscope depicts the load voltage, load current, compensating current, and calculates the current being drawn from the line by simply adding these two current waveforms.

4.4.2 Test Results

Fig. 4.4 demonstrate the result of the compensators for a non-periodic load resulted from a modeled $6.6Hz$ synchronous motor. For this purpose, the bandwidth reference (BW^*_{SC}) is set at $360Hz$ and the power rating ratio ($Ratio^*$) is set at 50% (0.5). The compensator parameters therefore, will be: $k = 0.11(40°)$, $SCALE = 0.63$, and $T = 9T_0$. It is noted that to fit the code into the maximum calculation window, it was necessary to perform the experiment in three steps:

- **Reactive Compensator:** In the first step, the reactive compensation of the load is performed with 12 kHz sampling frequency. After the compensation using the reactive compensator the remaining current is calculated (i_{RemRC}).

- **Fast Compensator:** In the second step, the generated remaining current (i_{RemRC}) is loaded to the fast compensator which is performing compensation with 18 kHz sampling frequency. The remaining current is treated by the compensator as it is the load current. Again, after the fast compensation the remaining current is calculated (i_{RemFC}).

- **Slow Compensator:** In the third step, the generated remaining current after the fast compensation (i_{RemFC}) is loaded to the slow compensator. The slow compensator samples the input current with 12 kHz sampling frequency. The remaining current is the line current which will be drawn from the grid.

The real-time results demonstrate that the modified version of the proposed compensator is capable of the compensation of the non-periodic current to an almost sinusoidal quantity. It is noted that the bandwidth of the fast compensator ($9kHz = 18kHz/2$) restricts the compensation of very high-frequency components of the current waveform. It is also pointed out that the line current will be ideally sinusoidal. However, since the slow compensator is assumed to have limited bandwidth (of $360Hz$) the final result of the line current will be less sinusoidal.

4.4.3 Code Optimization

Since for a real-time control application, the determinism (performing the whole code in a predetermined window of time) is crucial, the code should be optimized so that it takes the shortest deterministic possible time. The following considerations are taken to achieve the most optimum c code:

1. Using *double* data type proved to be more efficient than *float* due to the fact that the processor was 64 bit. Using *float* data type introduced some jitter to the code(variation of calculation period time from the desired deterministic maximum calculation window).

2. Preallocating the variables inside the memory largely decreases the jitter. For such purpose *static* variables are used.

3. Scaling the measurements to fixed-point and performing fixed-point calculation would not improve the code since the processor has the capability of hardware-based floating point calculation.

4. All the mathematical integrals are performed in a recursive manner. Doing so decreased the number of operations extensively. Moreover, any division that is possible to avoid was eliminated. For example, the equivalent conductance (equation (3.15)) is calculated as follows:

$$G_e(k) = \frac{P(k)}{V_1^2(k)} \tag{4.2}$$

Using the unoptimized code, the parameters are calculated as follows:

$$P(k) = \frac{\sum_{k=-N_T+1}^{0} p(k)}{N_T} \tag{4.3}$$

$$V_1{}^2(k) = \frac{\sum_{k=-N_T+1}^{0} v_1{}^2(k)}{N_T} \tag{4.4}$$

where N_T is number of calculation samples ($N_T = T.f_s$).

An optimize code, however, calculates these parameters as follows:

$$P(k) = P(k-1) + [p(0) - p(-N_T)] \tag{4.5}$$

$$V_1{}^2(k) = V_1{}^2(k-1) + [v_1{}^2(0) - v_1{}^2(-N_T)] \tag{4.6}$$

As a comparison, for the calculation of slow compensator equivalent conductance, the unoptimized code requires 3600 additions and 3 devisions; however, the optimized code only requires 2 additions and 2 subtractions and 1 devision.

5. Any unnecessary communication between the host machine and the real-time target shall be avoided. For example, releasing the code on the RT machine instead of establishing a debug between RT machine and the host increases the calculation speed up to t times.

4.5 Summary

This chapter is dedicated to the verification of the proposed tri-window compensator. The method is first verified using the simulation of real-world data acquired

from a local steel mill. It is shown that all the proposed power quality criteria would largely improve after the compensation using this compensator. Moreover, the method is further verified using real-time implementation of a controller-in-the-loop. The real-time implementation of the technique proved that the method is capable of removing the non-periodicity of the current. Note that the level of compensation of the sharp edges of the current is limited by the bandwidth of the fast compensator.

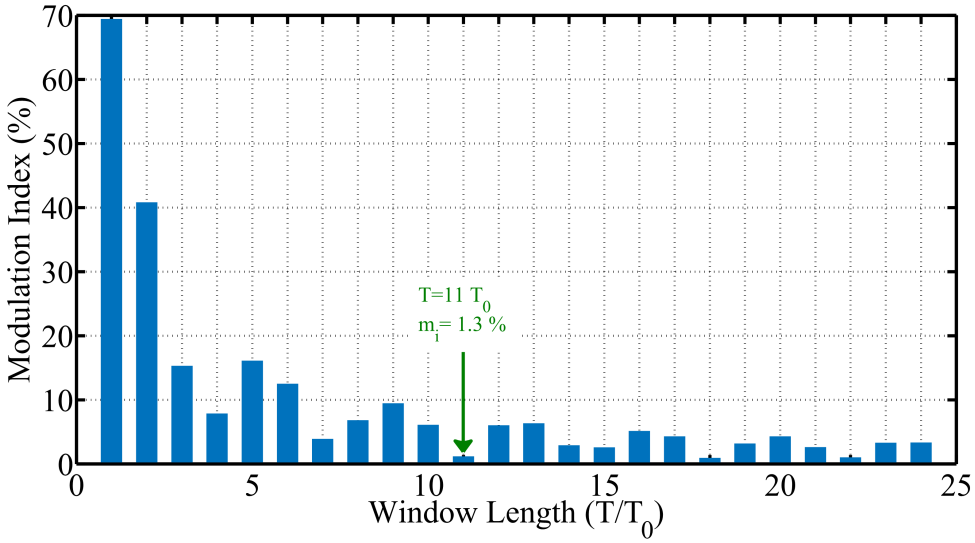

(a) Modulation index for different window lengths.

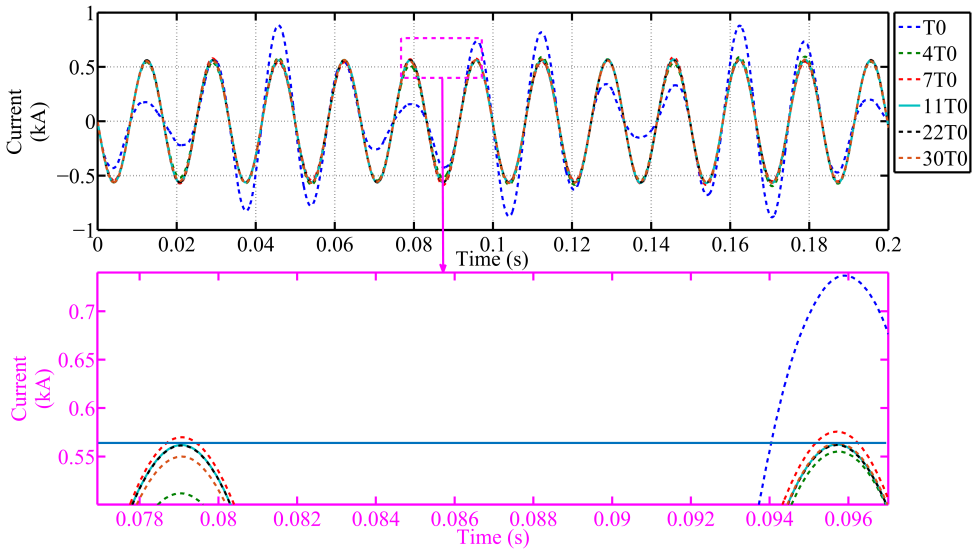

(b) Line current waveforms for different window lengths of the slow compensator.

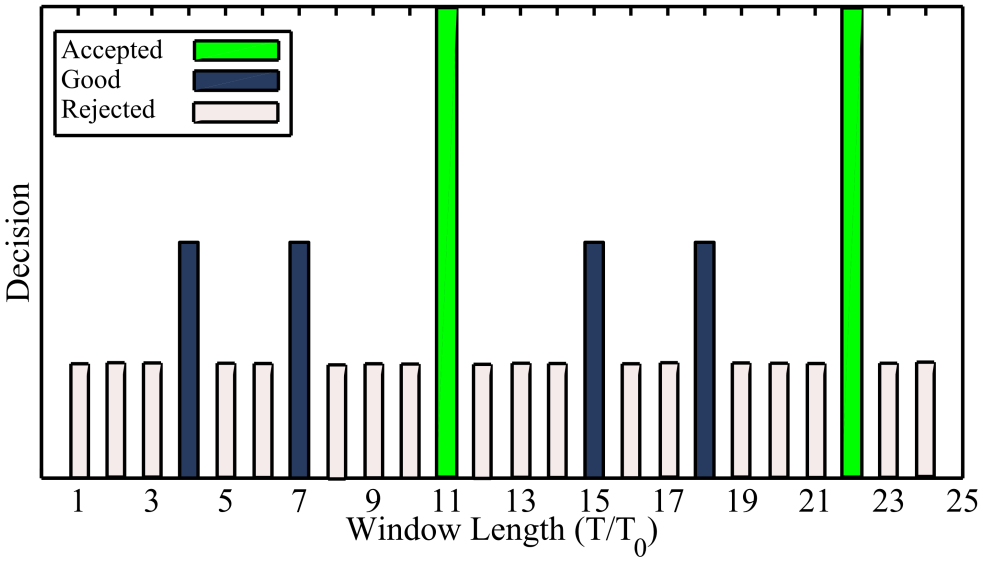

(c) Fuzzy logic decision for different window lengths of the slow compensator.

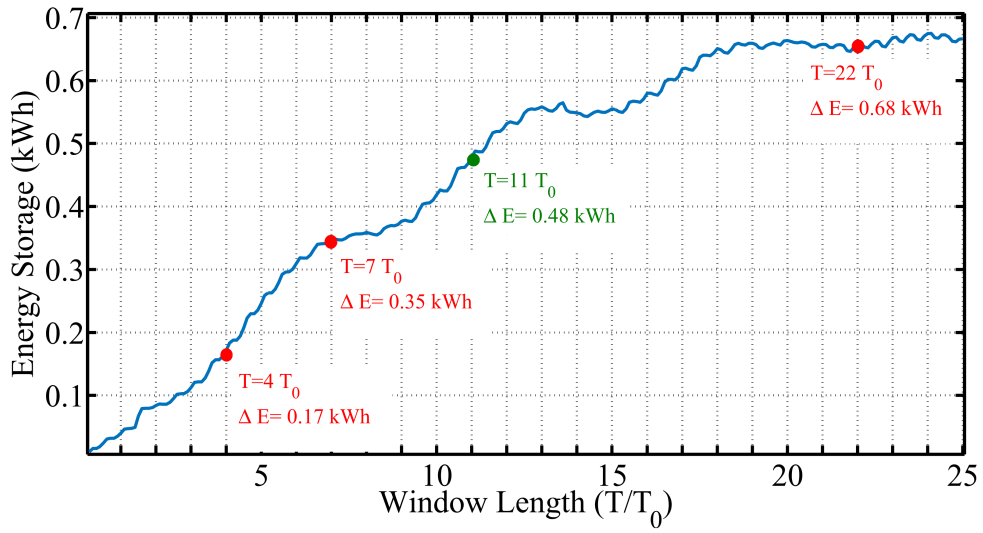

(d) Energy storage requirement for the slow compensator DC-link against the length of the calculation window.

Figure 4.3: Result of the slow compensator for loading *case* 1.

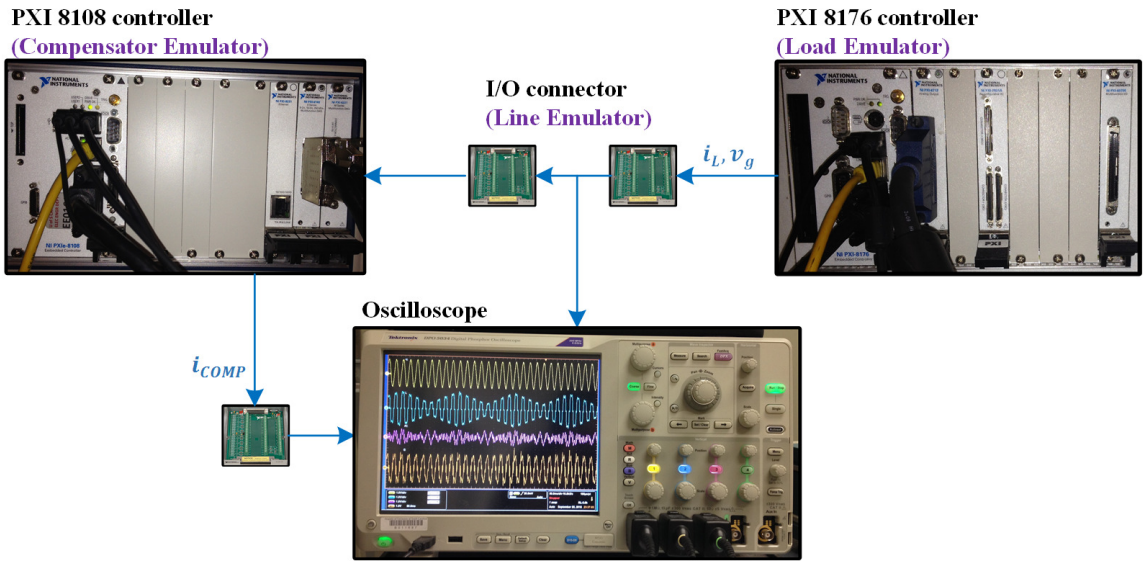

Figure 4.4: Real-time test setup schematic.

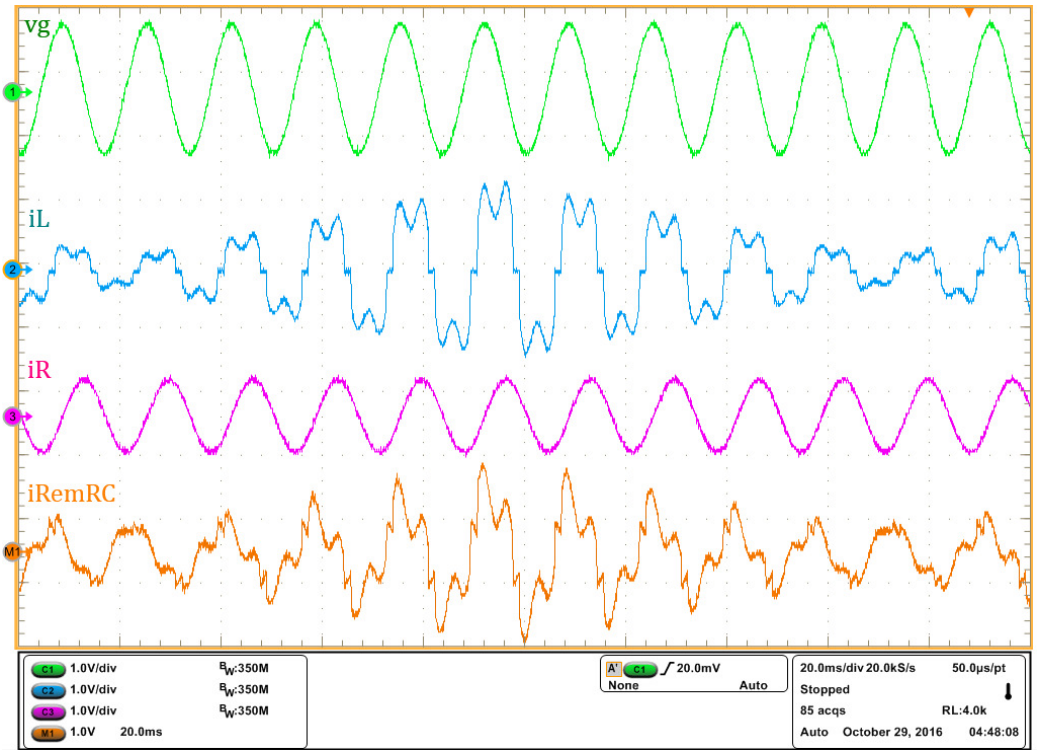

(a) Test result of the reactive compensator: (a) line voltage, (b) load current, (c) reactive compensator current, (d) remaining current after reactive compensation (i_{RemRC}).

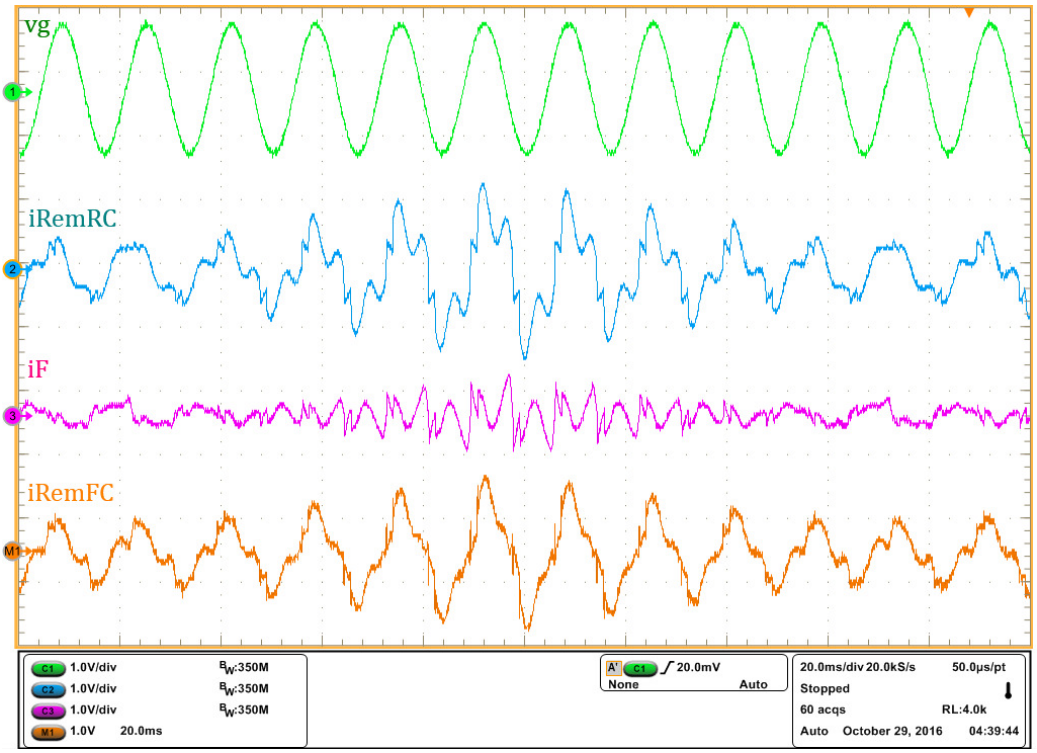

(b) Test result of the fast compensator: (a) line voltage, (b) remaining current after reactive compensation ($i_L = i_{RemRC}$), (c) fast compensator current, (d) remaining current after fast compensation (i_{RemFC}).

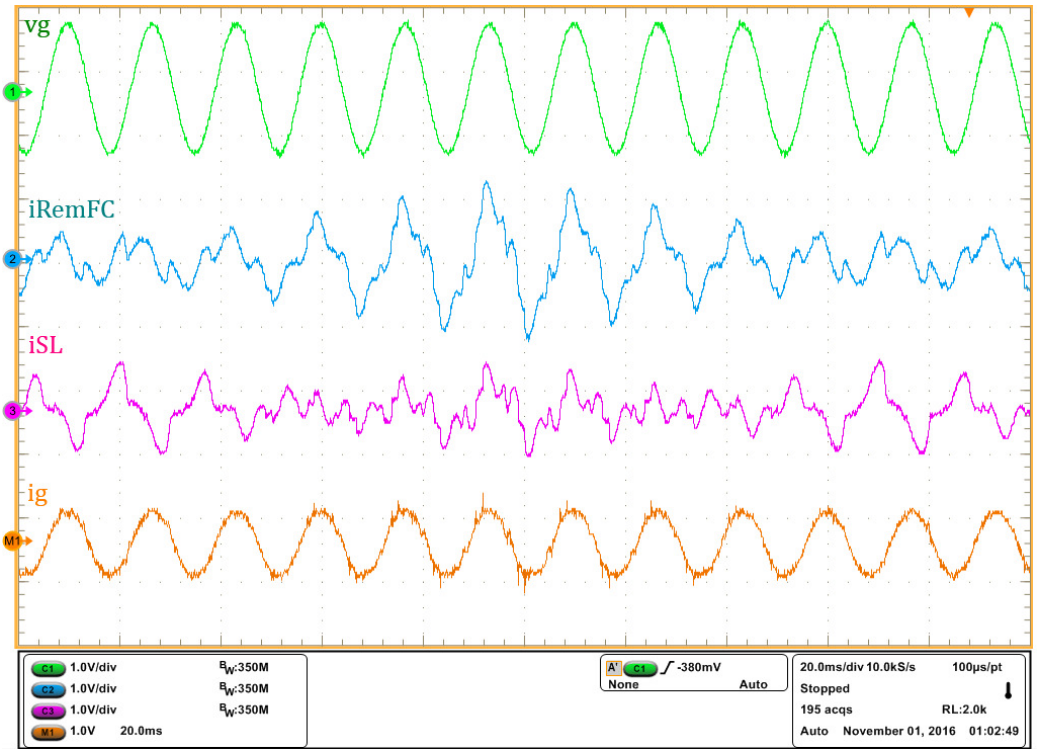

(c) Test result of the slow compensator: (a) line voltage, (b) remaining current after fast compensation ($i_L = i_{RemFC}$), (c) slow compensator current, (d) current drawn from the grid.

Figure 4.4: Test results.

Chapter 5

Practical Considerations

The desired real-time platform for testing and implementation of the tri-window compensator is shown in Fig. 5.1. In such design, the slow compensator and the non-periodic load can be implemented using two back-to-back power electronic building blocks (PEBBs). A PEBB is a three-phase bidirectional voltage source converter which, when accompanied by a proper control board, can function as a controlled current source. The fast compensator can also be implemented using only one PEBB.

The Energy Routing Laboratory of the University of South Carolina has the potential of developing a real-time test platform for the implementation of the tri-window compensator. However, the cost analysis of a Static VAR Compensator needs to be addressed before building the tri-window compensator.

5.1 Design and Cost Analysis of the Reactive Compensator (SVC)

The practical aspects of the Static VAR Compensator is required to be studied and analyzed to complete the design of the real-time platform used for the implementation of the tri-window compensator. The available power rating for the non-periodic load emulator is 35 kVA of which 16.4kVA is dedicated to the reactive power and 5.5 kVA is devoted to the unbalance power. There are several design factors that should be studied before building the SVC:

1. is the SVC responsible for compensating the unbalance power?

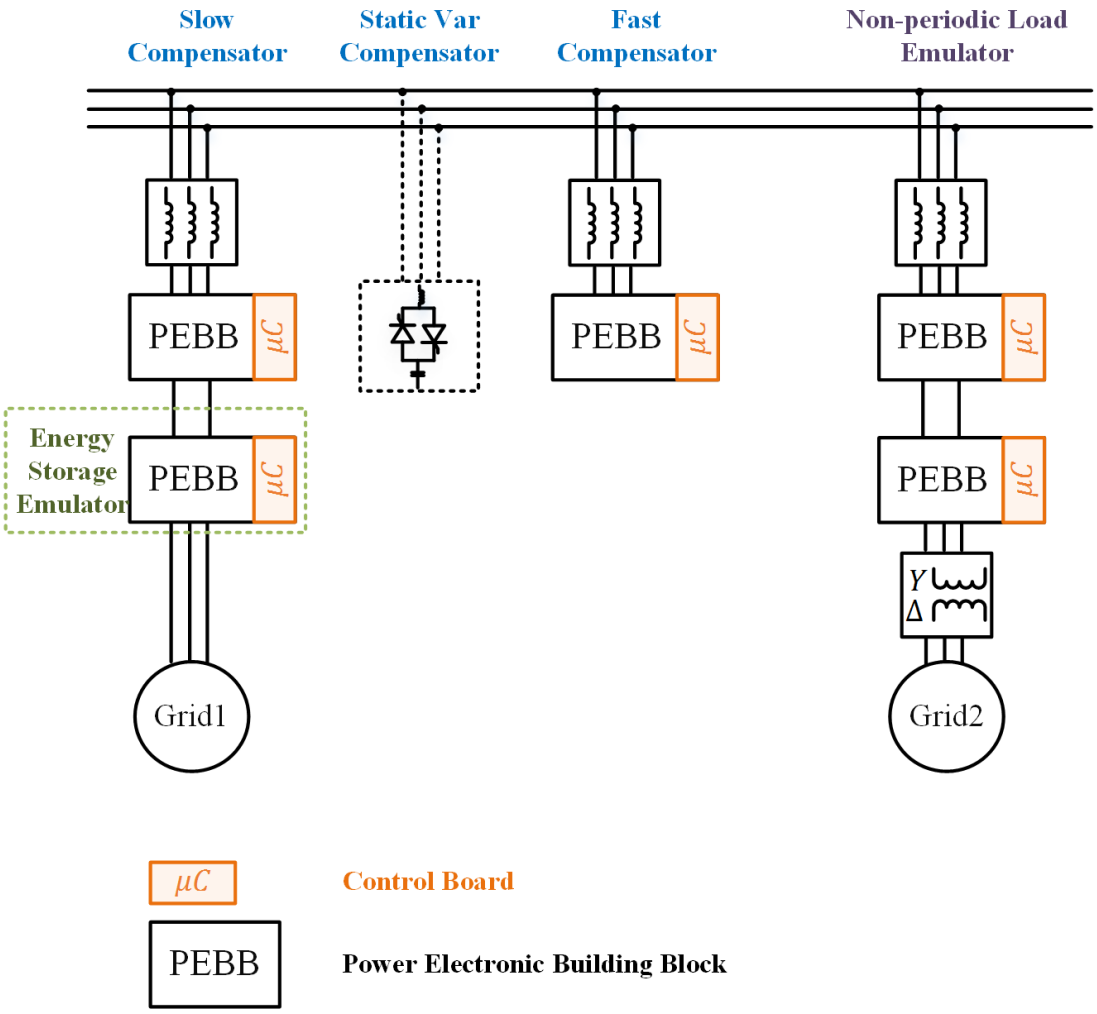

Figure 5.1: Desired real-time platform for development of the tri-window compensator.

2. which device is in charge of the compensation of harmonic byproducts of the reactive compensator?

Three SVC configurations are proposed, and cost analysis is performed to select the most optimum configuration. These three configurations are shown in Fig. 5.2.

The first option, FC-TCR (fixed capacitor- thyristor controlled reactor), shown in Fig. 5.2a is capable of compensating reactive power [25]. However, it generates current harmonics of the order $6k \pm 1$ multiples of the fundamental frequency. Moreover, this compensator is incapable of compensating the unbalance power. Therefore,

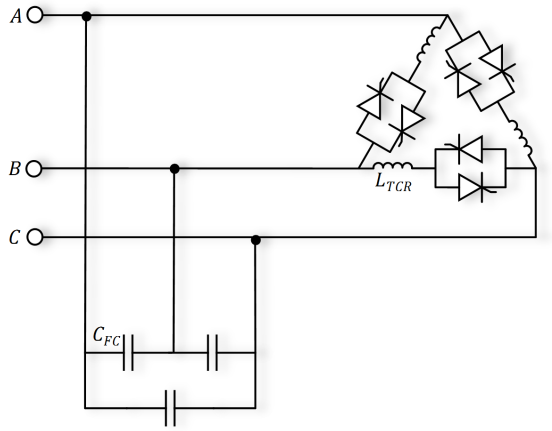

(a) Fixed capacitor thyristor controlled reactor (FC-TCR)

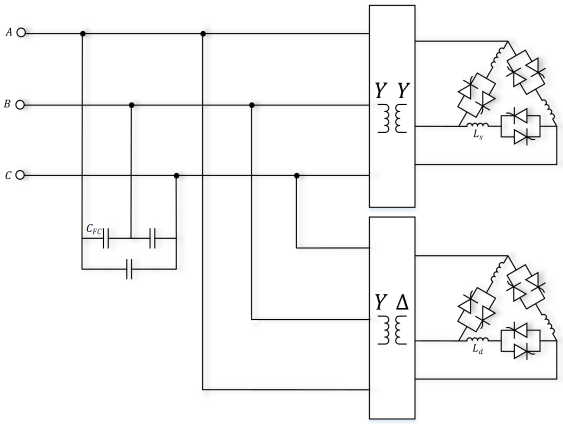

(b) Fixed capacitor 12-pulse thyristor controlled reactor.

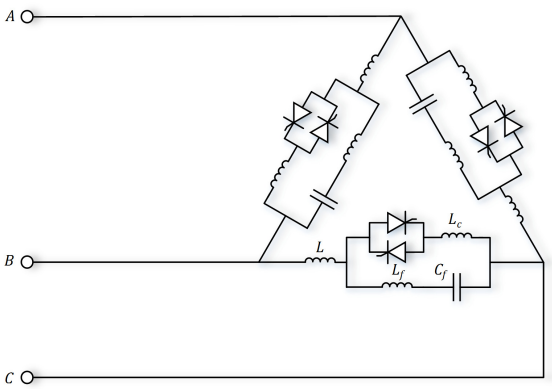

(c) Adaptive balancing compensator.

Figure 5.2: Static VAR Compensator designs used for performing cost analysis.

if the FC-TCR is used for the compensation of the reactive power, the slow compensator will be responsible for compensating the unbalance power and low-frequency harmonic byproduct of the reactive compensator. The fast compensator will also be responsible for compensating the high-frequency harmonic byproduct of the reactive compensator.

The second option, 12-pulse FC-TCR is shown in Fig. 5.2b. This device consists of one $Y-Y$ and one $Y-\Delta$ transformer that together reduces the harmonic content of the reactive compensator to $12k \pm 1$ multiples of the fundamental frequency [25]. However, similar to the basic FC-TCR, 12-pulse FC-TCR is incapable of compensating the unbalance power. Also, the additional transformers largely increase the cost of the design. Therefore, if the 12-pulse FC-TCR is used for the compensation of reactive power, the slow compensator will be responsible for compensating the unbalance power. Moreover, the fast compensator will be responsible for compensating the harmonic byproduct of the reactive compensator.

The third option, adaptive balancing compensator, is shown in Fig. 5.2c. This configuration is an extension of the FC-TCR that is also capable of compensating the unbalance part of the current [26]. However, since for the compensation of unbalance power the value of each phase to phase impedance should be different, the triple-nth harmonics generated by the TCR branch could not circulate inside the delta connected compensator and will be injected into the line. Therefore, although this compensator is capable of compensating the unbalanced power, it generates and injects $2k \pm 1$ multiples of the fundamental frequency to the grid. Thus, if this compensator is used for the compensation of the reactive power, its high power harmonic byproducts should be compensated using the fast and slow compensator.

A cost analysis has to be performed to select the optimum configuration based on the desired performance of the compensator and its power rating.

5.1.1 Cost Analysis of the SVC

Depending on the chosen SVC configuration, the size of the fast compensator and the size of the slow compensator increase. The reason is that the unbalance power, reactive power, and the harmonic byproduct of the compensator should be shared between the three compensators in the tri-window compensator structure. Therefore, the overall cost of the SVC design consists of the expense of the SVC configuration and the increase in cost (rating) of the fast and slow compensator. It is noted that instead of power rating, here we use the current RMS as the cost factor of the design. The reason is that, since the compensators are connected to the same terminals, they have equal voltage and therefore, the current RMS could be an indicator of the power rating. Therefore, the cost analysis of the SVC configuration is performed by minimizing the following cost function:

$$\lambda = I_F \times k_{FC} + I_{SL} \times k_{SC} + I_R \times k_{RC} \tag{5.1}$$

where λ is the overall cost in unit cost ($U\$$), I_F is the RMS current provided by the fast compensator to compensate the harmonic byproduct of the reactive compensator, I_{SL} is the RMS current provided by the slow compensator to compensate the unbalance power or harmonic byproduct of the reactive compensator. Additionally, k_{FC}, k_{SC}, and k_{RC} are the relative cost of the fast compensator, slow compensator, and reactive compensator in unit cost per unit current.

A parametric cost analysis of the SVC configuration is shown in Table 5.1. The value of the reactive current and the unbalance current is simply calculated by the required compensation rating (16.4 kVA for reactive load compensation and 5.5 kVA for unbalanced load compensation). Also, the harmonic byproducts of the SVC is calculated using the following equation for a single phase FC-TCR:

Table 5.1: Cost analysis of the Static VAR Compensator.

	Fast compensator (Relative cost k_{FC} [U$/A])		Slow Compensator (Relative cost k_{SC} [U$/A])		Static VAR Compensator			Cost
	Contribution	1-ph RMS current	Contribution	1-ph RMS current	Contribution	1-ph RMS current	Relative cost	
Balancing Compensator	Odd harmonics higher than 7th order	2.4 A	3rd, 5th, and 7th order harmonic	20.6 A	1)Reactive current 2)Unbalance current	47.9A	k_{ABC} [U$/A]	λ_{ABC} [U$]
Basic FC-TCR	$6k \pm 1$ harmonics higher than 7th order	0.8 A	1) 5th, 7th order harmonic 2) Unbalance current	15.5 A	Reactive current	45.5A	k_{BAS} [U$/A]	λ_{BAS} [U$]
12 pulse FC - TCR	$12k \pm 1$ harmonics higher than 7th order	0.4 A	Unbalance current	15.2A	Reactive current	45.5A	k_{12P} [U$/A]	λ_{12P} [U$]

$$I_{Ln}(\alpha) = \frac{V}{\omega_0 L}\frac{4}{\pi}\left\{\frac{sin(\alpha)\quad cos(n\alpha) - n\quad cos(\alpha)\quad sin(n\alpha)}{n(n^2-1)}\right\} \tag{5.2}$$

where I_{Ln} is the RMS value of the $n-th$ harmonic of the current, n is odd integer $(3, 5, 7, ...)$, α is the firing angle of the thyristor, V is the voltage across the TCR, ω is the frequency of the voltage waveform in (rad/s), and L is the value of inductor in the TCR branch.

For this cost analysis, the firing angle is set at $\alpha = 28.0$ degree to take into account the highest harmonic current generated by the TCRs.

The following relative cost factors are selected for each device: $k_{FC} = 1$, $k_{SC} = 1$, $k_{BAS} = 1$, $k_{12P} = 1.5$, and $k_{ABC} = 1.2$. This results in the following cost for each SVC structure: $\lambda_{BAS} = 61.8\ U\$$ for the FC-TCR, $\lambda_{12P} = 83.8\ U\$$ for the 12-pulse FC-TCR, and $\lambda_{ABC} = 80.6\ U\$$ for the adaptive balancing compensator. Therefore, it is apparent that using the basic FC-TCR as the SVC reduces the overall cost of the SVC design about $20 - 25\%$.

It is noted that the relative cost factor of the slow compensator and the fast compensator is dominated by the increase in the size of the output inductor. Moreover, if the relative cost of the basic FC-TCR is set as the reference, the cost of the adaptive balancing compensator increases mostly because of additional inductors, and the cost of 12-pulse FC-TCR increases mostly by the required six single-phase transformers.

Chapter 6

Toward Distributed Compensation: Power Quality Improvement inside Microgrids

If multiple active filters are needed for the compensation of power quality disturbances, two arrangements are possible, namely, distributed and co-located. Distributed arrangement has been widely used recently for the power quality disturbance compensation inside the microgrids [57]. For example, it has been used to compensate voltage harmonics and voltage imbalance in the grid-connected and islanded microgrids [58, 59, 60]. In this case, although active filters are distributed, they all use the same time-window size for the calculation of the reference signal. In other words, they are spatially distributed and temporally synchronized. The second arrangement of compensation devices, co-located, uses specific device for the compensation of each component of the current. For example, [50] proposed several devices for the compensation of all components of the disturbance current. Such techniques are also temporally synchronized. The tri-window compensator suggested in this dissertation is also co-located however since it uses different window length, it is temporally unsynchronized.

When it comes to microgrids (highly dispatchable load/generation units), however, since the active filter units (distributed generations) are distributed by nature, usage of co-located compensator structure is not possible. Moreover, the rapid growth of the non-linear and single phase loads in the microgrids pollutes the line current and voltage with harmonics and imbalance. Power transfer loss, interfere with sen-

sitive loads, stability issues, and a decrease in the microgrid efficiency are some of the consequences of this power quality disturbances. To eliminate these problems, the available rating of the distributed generations (DGs) in the microgrid could be exploited. In this chapter the current physical component (CPC) theory is utilized to generate a reference current for shunt active filters for harmonic/imbalance mitigation. Two set of droop controls, i.e. $G_h - \|i_h\|$ and $G_u - \|i_u\|$, are utilized to facilitates the sharing of the nonlinearity and asymmetry of the loads between different DGs. Moreover, a centralized controller connected with a low bandwidth communication line to the DGs is used to smooth out the total harmonic distortion and unbalance factor throughout the network.

The proposed technique, moreover, takes advantage of the combination of current physical component power theory and computationally effective recursive discrete Fourier transform (RDFT) for the calculation of the current reference. Therefore, the proposed technique has a low computational burden, due to the exploitation of RDFT and elimination of low pass- and high-pass filters. Also, the proposed technique can share the nonlinear and unbalanced load between different active filter units based on their available power rating.

6.1 Harmonic Node-Analysis of Microgrids

A typical grid-connected microgrid (MG) is demonstrated in fig. 6.1. MGs often consist of various energy resources, such as solar cells, fuel cells, wind turbines, and energy storage systems. Non-linear loads such as electric vehicles and residential loads could also be inside to the MGs. Since these sources and loads are mostly connected to the microgrid through power electronics based converters, the microgrid could become highly polluted with power quality disturbances, such as harmonics, unbalanced current, and reactive power. The elimination of power system polluting current is critical as it largely decreases the efficiency of the microgrid.

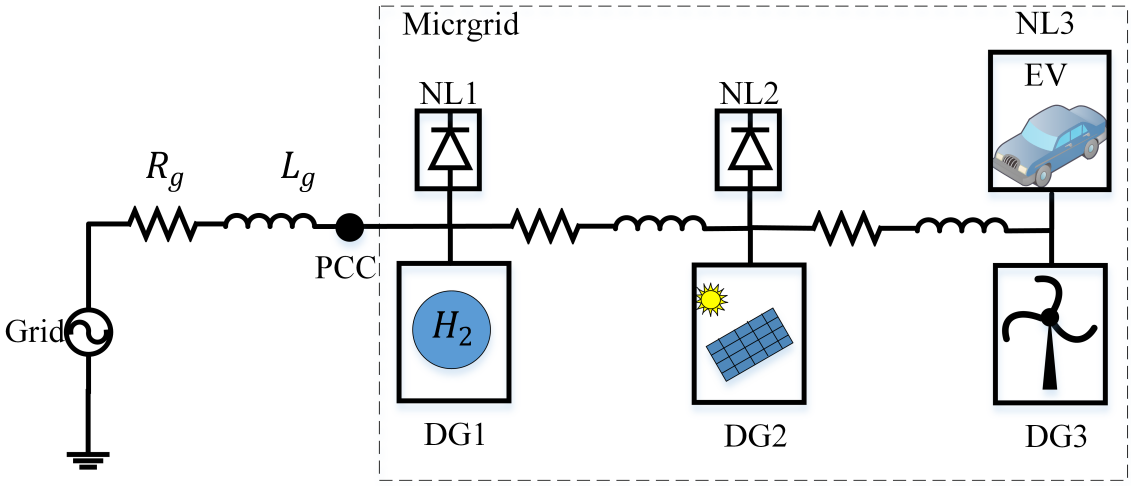

Figure 6.1: Typical microgrid structure with fuel cell, photovoltaic, and wind turbine generation, and electric vehicle and other non-linear loads.

In this section, the voltage harmonic compensation in the microgrid is discussed using the node analysis. The two-node equivalent circuit of the microgrid for harmonic frequencies is shown in fig. 6.2a. To simplify the analysis, assume that the length of the distribution line is less than a tenth of the highest compensated frequency wavelength in the network. Therefore, the lines could be safely modeled as resistance in series with the inductance. Moreover, the series compensator is presented using its equivalent virtual resistance (frequency-dependent), and the distorted grid and the non-linear load are demonstrated using harmonic current sources. The two-node structure is proper for the voltage compensation analysis, as it could help studying both the harmonic propagation to remote nodes (RN), and harmonic pollution of the point of common coupling (PCC). A more simplified version of this circuit is shown in fig. 6.2b. The harmonic voltage of two nodes could be calculated using the node analysis as follows:

$$\begin{bmatrix} I_{h1} \\ I_{h2} \end{bmatrix} = \begin{bmatrix} Y_1 + Y_L & -Y_L \\ -Y_L & Y_2 + Y_L \end{bmatrix} \begin{bmatrix} V_1 \\ V_2 \end{bmatrix} \tag{6.1}$$

Using the matrix inverse transform, the harmonic voltage at the PCC and the

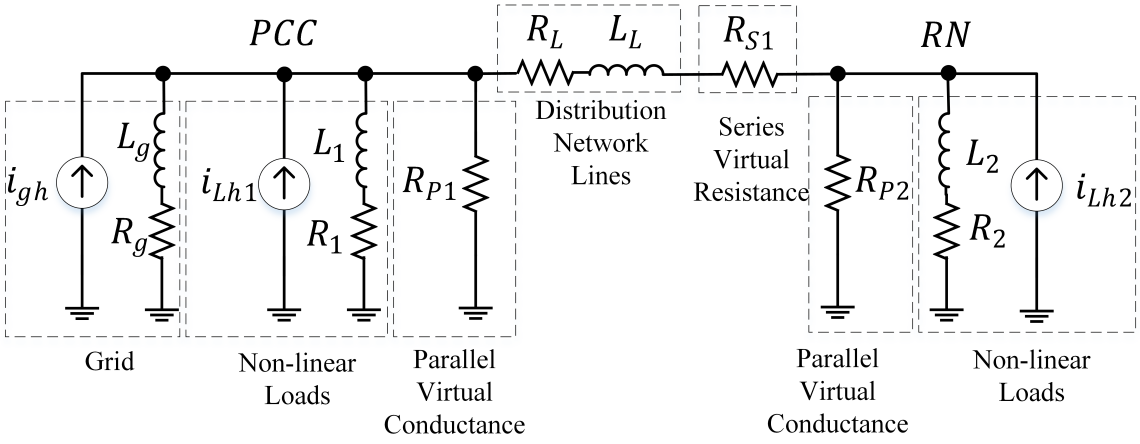

(a) Equivalent circuit of the grid connected microgrid.

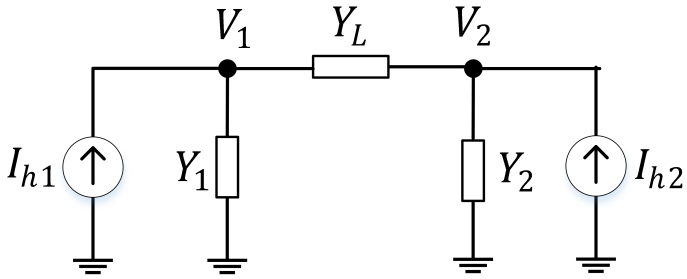

(b) Simplified equivalent circuit of the grid connected microgrid.

Figure 6.2: The node-analysis representation of the grid connected microgrid

RN is calculated as follows:

$$\begin{bmatrix} V_1 \\ V_2 \end{bmatrix} = \begin{bmatrix} Z_{11} & Z_{12} \\ Z_{21} & Z_{22} \end{bmatrix} \begin{bmatrix} I_{h1} \\ I_{h2} \end{bmatrix} \tag{6.2}$$

where Z_{11}, $Z_{12}(= Z_{21})$, and Z_{22} are the arrays of the admittance inverse matrix, not to be confused with impedance matrix used for mesh analysis, and are calculated as follows:

$$Z_{11} = \frac{Y_2 + Y_L}{(Y_1 + Y_L)(Y_2 + Y_L) - {Y_L}^2} \tag{6.3}$$

$$= \frac{Y_2 + Y_L}{Y_1 Y_2 + (Y_1 + Y_2) Y_L} \tag{6.4}$$

$$Z_{22} = \frac{Y_1 + Y_L}{(Y_1 + Y_L)(Y_2 + Y_L) - {Y_L}^2} \tag{6.5}$$

$$= \frac{Y_1 + Y_L}{Y_1 Y_2 + (Y_1 + Y_2) Y_L} \tag{6.6}$$

$$Z_{12} = Z_{21} = \frac{Y_L}{(Y_1 + Y_L)(Y_2 + Y_L) - {Y_L}^2} \tag{6.7}$$

$$= \frac{Y_L}{Y_1 Y_2 + (Y_1 + Y_2) Y_L} \tag{6.8}$$

It could be concluded from the eq. (6.3) that in order to minimize the voltage harmonics on each node, two options are available; decreasing the diagonal impedances (Z_{11} and Z_{22}), or decreasing the off-diagonal impedances (Z_{12} and Z_{21}). The diagonal arrays are responsible for the voltage harmonics that are result of the non-linear loads at the same node. On the other hand, the off-diagonal arrays are responsible for the harmonic propagation. First, let's analyze minimizing the diagonal impedances, e.g. Z_{11}.

The minimization of Z_{11} is achievable by installing a parallel virtual impedance, $G_{p1}(= 1/R_{p1})$, at the PCC, which increases Y_1. However, increase or decrease in Y_L and Y_2 does not necessarily contribute to the minimization of Z_{11}. Therefore, the voltage harmonics due to the non-linear load on the node it is connected to could only be eliminated using parallel virtual impedance (providing parallel current path).

The minimization of the off-diagonal arrays, e.g. Z_{12}, could be achieved by installing parallel virtual impedances, G_{p1} and G_{p2}, or installing series virtual impedance, R_{S1}, which decreases Y_L. Therefore, the harmonic propagation could be blocked using both series and parallel virtual impedances. It is noted that in typical distribution systems without compensation, the line impedance is way smaller than the load impedances ($Y_L >> Y_1$ and $Y_L >> Y_2$).

To sum up, there are two directions for decreasing the voltage harmonics throughout the network; (1) providing a parallel path for the harmonic current at each node

(nodal compensation), and (2) blocking the harmonic propagation at each line (loop compensation). The late goal could be achieved using the well-known shunt virtual conductance, while the latter would be accomplished by both the parallel virtual conductance and the series virtual resistance, which is proposed in this chapter. Although the shunt compensation has attracted more interest in harmonic compensation, it needs high rating active power filters for blocking the harmonic propagation. Therefore, the proposed technique in this work is to prevent the harmonic propagation throughout the network by using virtual series resistance whose magnitude is controlled using a droop controller for equivalent sharing of the voltage harmonics between different active filters.

6.2 Fundamental of Voltage Compensation

6.2.1 Current Physical Components Theory for Harmonic and Imbalance Current Extraction

Czarnecki [61, 62] proposed a frequency domain approach for the extraction of reactive, unbalanced, and harmonic components of the current. In [63], the method is further improved using the computationally practical recursive discrete Fourier transform (RDFT) for the calculation of the fundamental frequency component.

Assume three-phase load current and line voltage are measured at the terminals of the active power filter are $\{i_R, i_S, i_T\}$ and $\{v_R, v_S, v_T\}$. It is shown in [63] that in three phase and three wire systems the measurement of two-phase (R and S) is enough for the compensation purposes. The reason is that the third voltage and current quantity is linearly dependent on the other two quantities.

In this section the extended current physical component (CPC) technique is used for the extraction of harmonics from the current waveform. The CPC method de-

composes the phase current, i, into four components:

$$i = i_a + \underbrace{i_r + i_u + i_h}_{i_c} \tag{6.9}$$

where i_a is the active current which is the part of the current responsible for the transfer of active power toward the load; i_c is the non-active part of the current which is required to be compensated to assure high power quality and consists of reactive, unbalanced, and harmonic current; i_r is the reactive current, which transfers the reactive power; i_u is the unbalanced part of the current, whose compensation results in balanced power being drawn from the source; and i_h is the harmonic part of the current. These four components are proved to be mutually orthogonal which allows their independent compensation.

In order to perform the CPC decomposition, each of the aforementioned current components should be calculated. The first step toward this calculation is calculating the time varying equivalent admittance of the load, $\tilde{Y}_e(= \tilde{G}_e + j\tilde{B}_e)$, which is calculated as follows:

$$\tilde{Y}_e = \tilde{Y}_{ST} + \tilde{Y}_{TR} \tag{6.10}$$

$$\tilde{Y}_{TR} = \frac{\tilde{I}_R}{\tilde{U}_{RT}}, \tilde{Y}_{ST} = \frac{\tilde{I}_S}{\tilde{U}_{ST}} \tag{6.11}$$

where $\{\tilde{I}_R, \tilde{I}_S\}$ and $\{\tilde{U}_{RT}, \tilde{U}_{ST}\}$ are the fundamental harmonic phasor of line current and line-line voltage, respectively.

Moreover, the time-varying unbalanced admittance which is used for the unbalanced current compensation is defined as follows:

$$\tilde{A} = \left|\tilde{A}\right| e^{j\tilde{\varphi}} = (\tilde{Y}_{ST} + \alpha\tilde{Y}_{TR}) \tag{6.12}$$

where $\alpha(= e^{j120})$ is used to decompose the unbalanced currents to three balanced components.

Using the equivalent admittance and unbalanced admittance, the active current, reactive current, and unbalanced current could be found as follows:

$$i_a = \begin{bmatrix} i_{Ra} \\ i_{Sa} \end{bmatrix} = \sqrt{2}\tilde{G}_e \begin{bmatrix} Re\{\tilde{U}_R\} & -Im\{\tilde{U}_R\} \\ Re\{\tilde{U}_S\} & -Im\{\tilde{U}_S\} \end{bmatrix} \begin{bmatrix} cos(\omega_{1g}k) \\ sin(\omega_{1g}k) \end{bmatrix} \tag{6.13}$$

$$i_r = \begin{bmatrix} i_{Rr} \\ i_{Sr} \end{bmatrix} = -\sqrt{2}\tilde{B}_e \begin{bmatrix} Im\{\tilde{U}_R\} & Re\{\tilde{U}_R\} \\ Im\{\tilde{U}_S\} & Re\{\tilde{U}_S\} \end{bmatrix} \begin{bmatrix} cos(\omega_{1g}k) \\ sin(\omega_{1g}k) \end{bmatrix} \tag{6.14}$$

$$i_u = \begin{bmatrix} i_{Ru} \\ i_{Su} \end{bmatrix} = \tag{6.15}$$

$$\sqrt{2} \begin{bmatrix} Re\{\tilde{A}\}Re\{\tilde{U}_R\} - Im\{\tilde{A}\}Im\{\tilde{U}_R\} & -(Re\{\tilde{A}\}Im\{\tilde{U}_R\} + Im\{\tilde{A}\}Re\{\tilde{U}_R\}) \\ Re\{\tilde{A}\}Re\{\tilde{U}_T\} - Im\{\tilde{A}\}Im\{\tilde{U}_T\} & -(Re\{\tilde{A}\}Im\{\tilde{U}_T\} + Im\{\tilde{A}\}Re\{\tilde{U}_T\}) \end{bmatrix}$$

$$\times \begin{bmatrix} cos(\omega_{1g}k) \\ sin(\omega_{1g}k) \end{bmatrix}$$

where $Re(X)$ and $Im(X)$ reflect the real and imaginary components of phasor X.

The fourth component of the current waveform, the harmonic component, is calculated simply by subtracting the active, reactive, and unbalance current from the current waveform. This is a critical property of the CPC method since it only requires working on fundamental frequency components and there is no need for additional filtering to calculate the harmonic part of the current.

$$i_h = i - (i_a + i_r + i_u) \tag{6.16}$$

A flexible active compensator could be realized by adaptively compensating each component of the current waveform [63]. Using this technique, the compensator current, i_C, is not equal to the disturbance current ($=i_r + i_u + i_h$). Instead, the part of the current which has higher priority for the compensation could utilize more of the rating power of the compensator. Therefore, the current reference of the active compensator becomes equal to:

$$i_c^* = M_r i_r + M_u i_u + M_h i_h \tag{6.17}$$

where M_r,M_u, and M_h are the weight coefficients for reactive, unbalanced, and harmonic current on the output.

In the next step of the reference generator, the shunt current reference is calculated. Its value is equal to the multiplication of the harmonic voltage, U_h, by a droop-derived virtual conductance, G_h, plus multiplication of the harmonic voltage, U_u, by a droop-derived virtual conductance, G_u. Therefore, based on the discussion in section 6.1, the active filter will behave as virtual conductance for both voltage harmonics and voltage unbalance and could dampen the effect of voltage disturbance. The reference current of the active filter will be:

$$j^* = G_h u_h + GuU_u \tag{6.18}$$

The droop control is a higher control structure, used as a sharing scheme between multiple distributed active filters throughout the microgrid. This control technique permits sharing the distortion part of the load between different active filters proportional to their available power rating [64]. The value of the virtual conductances, therefore, are calculated as follows:

$$G_{h_i} = G_{h_{i0}} + b_{h_i}(S_i - H_i - U_i) \tag{6.19}$$

$$G_{u_i} = G_{u_{i0}} + b_{u_i}(S_i - H_i - U_i) \tag{6.20}$$

where i reflects the ith active filter, $G_{h_{i0}}$ and $G_{u_{i0}}$ are the rated conductances, S reflects the available apparent power of the compensator, and H reflects the harmonic power, and U reflects the unbalance power, calculated as follows:

$$P^2 = \|V_{AF}\|^2\|I_a\|^2, \quad Q^2 = \|V_{AF}\|^2\|I_r\|^2 \tag{6.21}$$

$$H^2 = \|V_{AF}\|^2\|I_h\|^2, \quad U^2 = \|V_{AF}\|^2\|I_u\|^2 \tag{6.22}$$

$$S^2 = S_0^2 - P^2 - Q^2 - U^2 - H^2 \tag{6.23}$$

where S_0, P, Q, U, and H reflect the active filter rated power, active power, reactive power, unbalanced power, and harmonic power, respectively. Moreover, $\|X\|$

demonstrate the norm of the signal, x, calculated using the inner product function as follows:

$$\|X\|^2 = \frac{1}{T}\int_0^T x(t)^2 dt \tag{6.24}$$

where T is the period of the periodic signal, x. The structure of the proposed current reference calculator is shown in Fig. 6.3. There is another higher level control structure in this figure which is used to further smooth out the microgrid harmonic and imbalance. The purpose of this centralized controller is to keep the average voltage THD and average voltage unbalance factor (equation (1.3)) within acceptable region. This is performed by manipulating the droop slope of the controllers (b_{h_i}, b_{u_i}).

6.2.2 Recursive Discrete Fourier Transform (RDFT)

In this section, the RDFT is used for the calculation of voltage and current phasors, (U_{S1}, U_{R1}) and (I_{S1}, I_{R1}). The frequency response of the RDFT is shown in Fig. 6.4, where H_C, H_S, H are the magnitude of cosine filter, sine filter, and total filter, respectively. It is evident from the figure that, as long as no non-integer multiplication of fundamental frequency exists in the frequency spectrum (as of the case of non-periodic current), the RDFT returns the magnitude of the fundamental frequency with zero error. The fundamental frequency phasor X_1 of the sampled signal $x(n)$ is calculated using DFT (discrete Fourier transform) as follows:

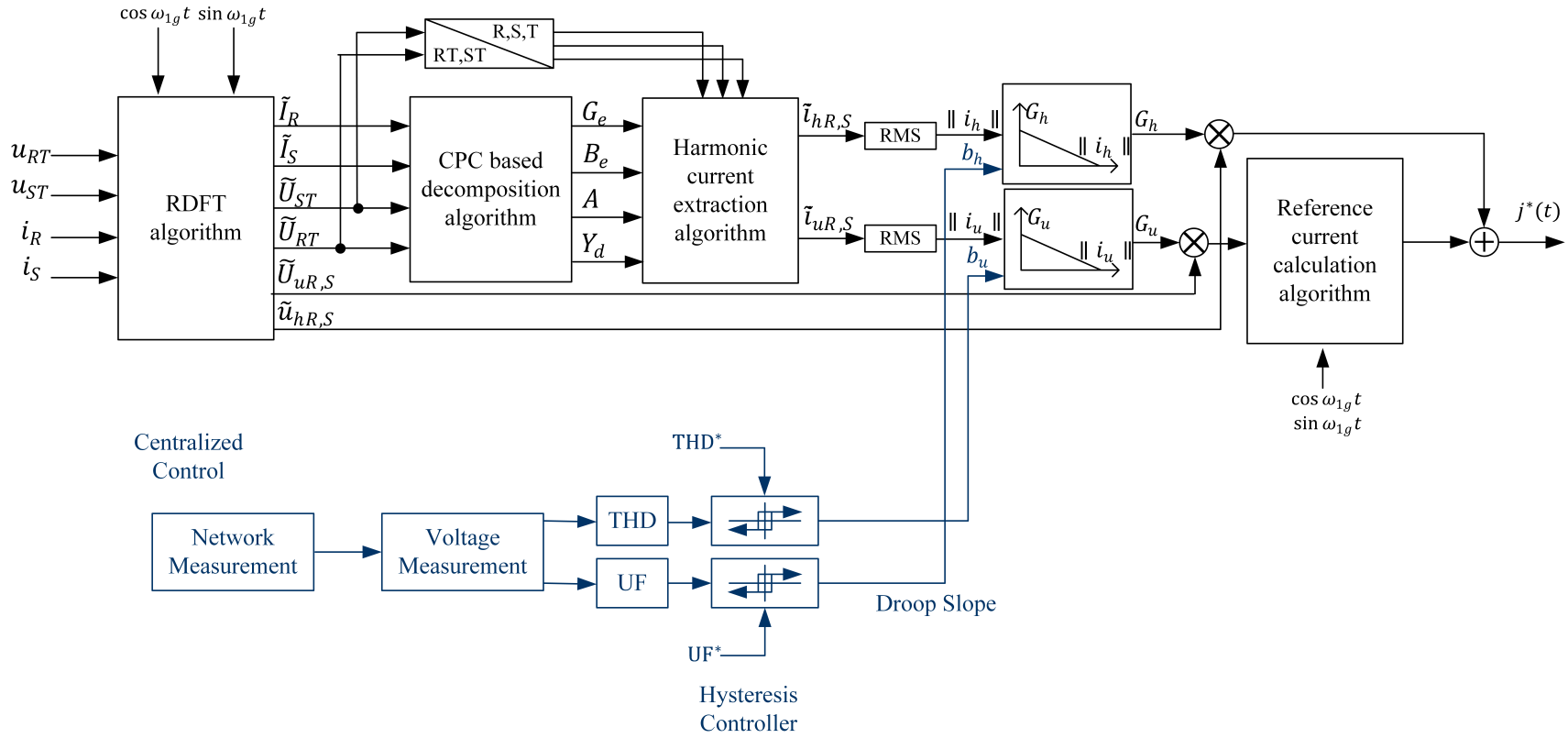

Figure 6.3: Structure of the proposed shunt harmonic and unbalance compensation technique.

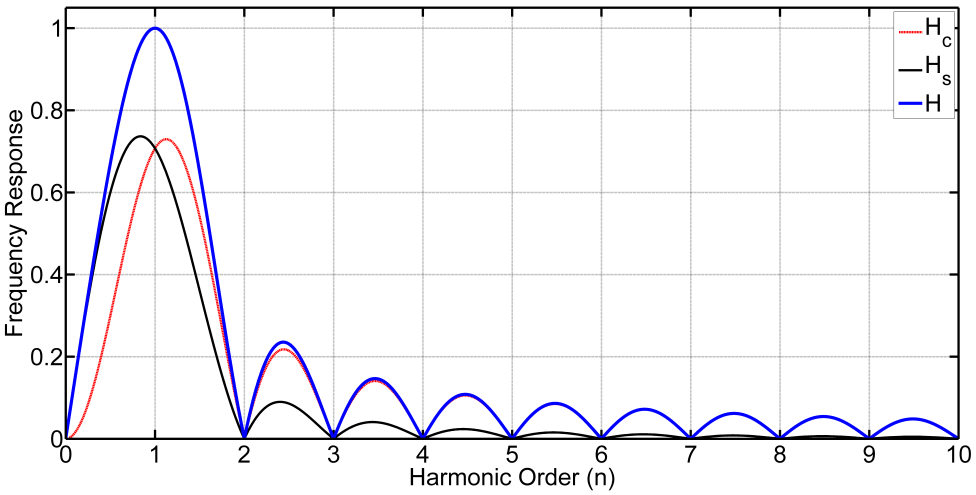

Figure 6.4: The frequency response of the proposed RDFT filter.

$$\tilde{X}_{1C} = \frac{\sqrt{2}}{N} \sum_{i=0}^{N-1} x(i+k-N+1) cos(\omega_{1g} i) \tag{6.25}$$

$$\tilde{X}_{1S} = -\frac{\sqrt{2}}{N} \sum_{i=0}^{N-1} x(i+k-N+1) sin(\omega_{1g} i) \tag{6.26}$$

$$\tilde{X}_1 = \tilde{X}_{1C} + \tilde{X}_{1S} \tag{6.27}$$

where the subscript $1C$ and $1S$ represent the cosine- and sine-filtered fundamental harmonic. Moreover, the " ˜ " demonstrated that the value of the phasor is calculated through the sliding window DFT. The RDFT is the recursive form of the DFT, which reduces the number of arithmetic operations to only two additions, two multiplications, and two subtractions in each calculation time interval. Therefore, RDFT largely increases the calculation speed of the fundamental frequency components, especially when the sampling rate is high. Moreover, the RDFT has a faster dynamic to reach the steady state value. The RDFT is calculated as follows:

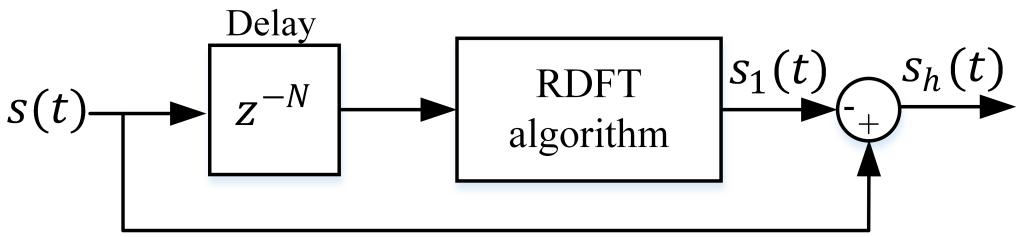

Figure 6.5: The filter for the extraction of the voltage harmonic.

6.3 System Under Study

The result of the proposed technique is analyzed using the circuit proposed in [65]. A Matlab block diagram of this system is shown in Fig. 6.6.

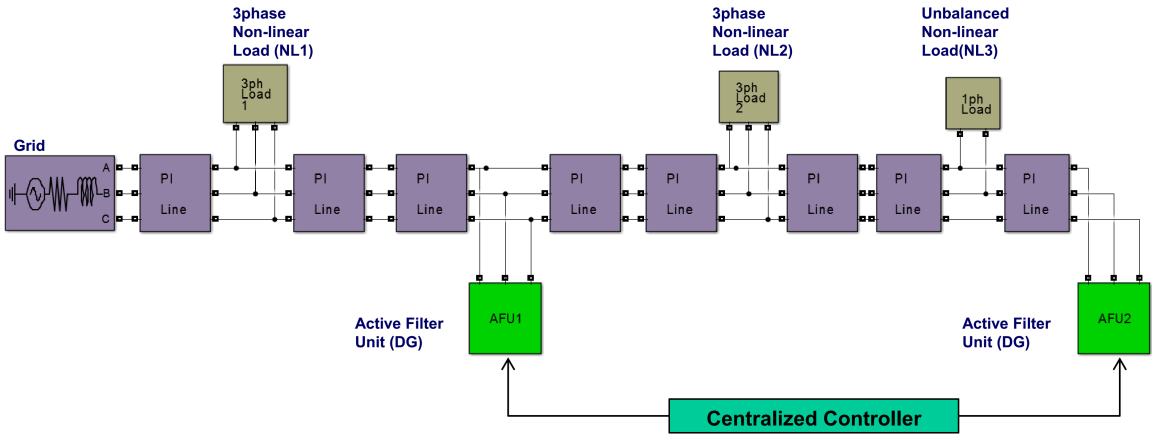

Figure 6.6: Schematic of the system under study used to test the proposed technique

Moreover, the loading scheme shown in Fig. 6.7 is used to activate different active filters and loads.

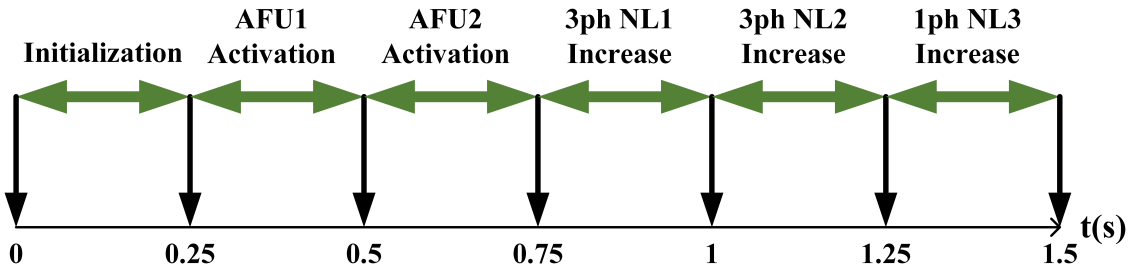

Figure 6.7: The time-line of different events in the simulation.

6.4 Results and Discussion

In this section the product of the proposed technique is demonstrated and compared with two conditions: (1) un-compensated microgrid, (2) microgrid compensated with distributed compensation without centralized THD and UF controller. Fig. 6.8 demonstrate the variation of two power quality factors, THD and UF, for these three conditions. It is noted that the THD and UF references are set at 3% for this study. Without using an active filter, the value of THD increases by any addition of non-linear load. UF also increases by the introduction of single phase load. However, using both cases of active filter (centralized and distributed) largely decreases the value of these power quality criteria. Moreover, when these criteria are outside of their required band ($< 3\%$), the centralized controller behaves better by pushing the value of them further down.

Moreover, it is important to understand that using the centralized method, though brings smoother power quality criteria, increases the required power rating of the compensators. This is shown in Fig. 6.9. Moreover, this technique completely relies on the existence of low bandwidth reliable communication from the nodes in the microgrid to the control center and from the control center to the active filters.

6.5 Future Work

This chapter was dedicated to the preliminary study of a distributed control structure for the mitigation of the microgrid unbalance and harmonic voltage. The proposed technique combines the CPC and RDFT to develop a droop controlled virtual resistance for the distributed active filters. Also, a centralized controller is used for smoothing the THD and UF throughout the network, while optimizing the energy consumption. When the THD and UF are out of the accepted region, the centralized hysteresis based controller increases the output current of the AFUs to move

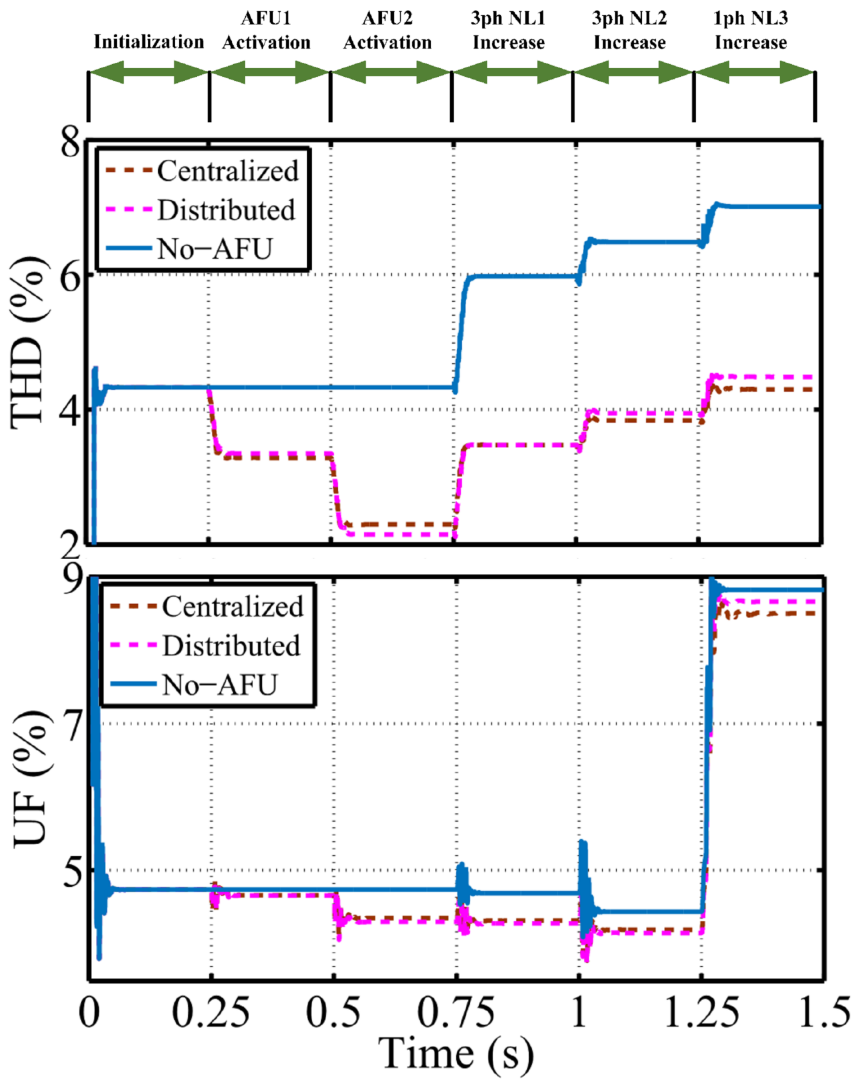

Figure 6.8: Power quality criteria, without compensation, with compensation by distributed control, and with compensation by centralized control

the system back to an acceptable operating point. The proposed scheme not only facilitates sharing of imbalance and harmonic load but also adaptively optimizes the disturbance power generation.

In spite of these advantages, the proposed technique still requires further study. The following steps are ahead of this research for further improvement:

1. Developing the proposed technique to improve the power quality in more challenging scenarios, such as asymmetric supply voltage and poly-phase systems

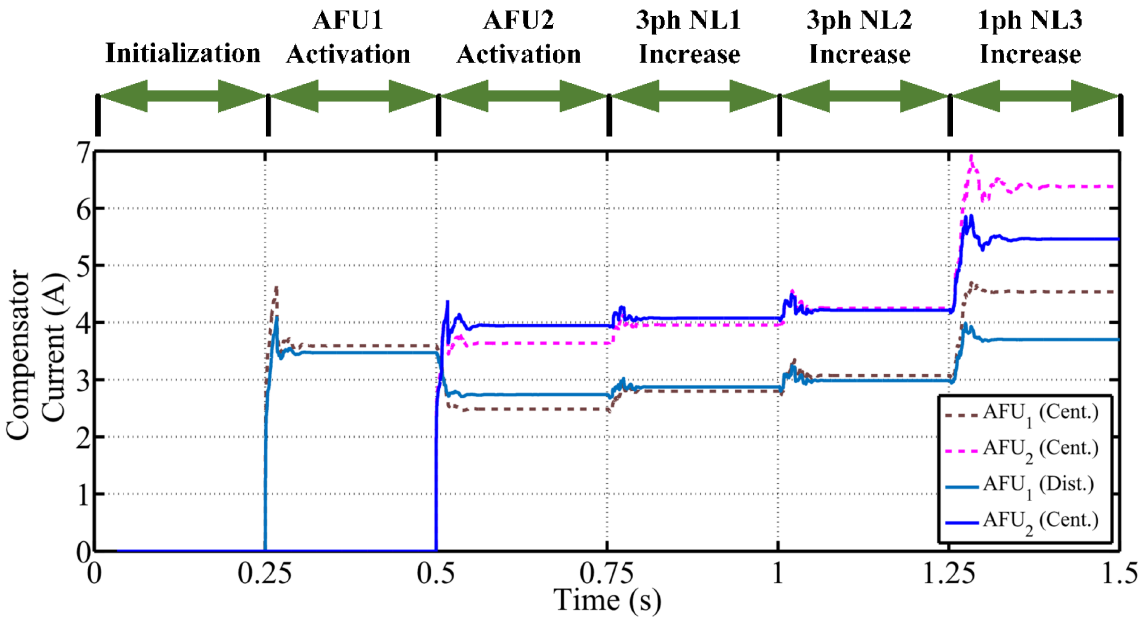

Figure 6.9: The RMS current of the active filter units with and without the centralized controller.

2. Developing distributed series and distributed hybrid compensators and comparing them with the original shunt compensator

3. Designing new adaptive control algorithm to adaptively change the controller setting for large variations in the load current frequency spectrum and asymmetry

4. Evolving the method toward the load compensation and power quality disturbance sharing in the stand-alone Microgrids

5. Testing the method using the real-time simulation

6. Evaluating the method using real-world setup of the Microgrid,

Chapter 7

Conclusion

A novel tri-window based compensator for the compensation of loads with a non-periodic current was proposed. This compensator consists of three co-located devices with different calculation window, called fast compensator, reactive compensator, and slow compensator. By decomposing the load current into mathematically non-orthogonal non-synchronized components, different frequency ranges of the current waveform are addressed separately. This optimizes the design of active filters, by choosing devices with lower power rating and higher switching frequency, and devices with higher power rating and lower switching frequency. Moreover, separating the reactive current component of the load current allows utilizing the Static Var Compensators (SVCs) which lowers the overall cost of the design. Adding an adaptive fuzzy algorithm, whose rules are based on the characteristics of the non-periodic loads, results in optimizing the window length of the slow compensator and decreasing bandwidth and reaction time of the compensator to transients.

Three power quality criteria, named time-frequency distortion index ($TFDI$), high-frequency distortion index ($HFDI$) and modulation index (m_i), capable of describing the behavior of non-periodic current compensator, were proposed. These indices are used to evaluate the proposed technique and also as a supervisory control of the design.

The verification of the proposed technique was performed with the simulation and real-time structure. The method was first verified using the simulation of real-world data acquired from a local steel mill. It was shown that all the proposed power

quality criteria would largely improve after the compensation using this compensator. Moreover, the method was further verified using real-time implementation of a controller-in-the-loop. The real-time implementation of the technique proved that the technique was capable of removing the non-periodicity of the current.

One of the challenges with the proposed method was that, though the reactive compensator current and slow compensator currents are mathematically orthogonal, the fast compensator current is not orthogonal to them. However, since these components are sequentially ordered, the orthogonality requirement is waived.

In the last chapter of this dissertation, the possible road toward the distributed structure for the compensators is discussed. Moreover, preliminary study of a distributed structure with a centralized higher level control is performed, and the preliminary results demonstrate a high capability of this structure. This chapter opens up research potential for further investigation of power quality improvement using the advanced digital signal processing and the power electronics.

Bibliography

[1] R. C. Dugan, M. F. McGranaghan, and H. W. Beaty, "Electrical power systems quality," *New York, NY: McGraw-Hill,/ c1996*, vol. 1, 1996.

[2] F. G. Montoya, A. GarcÃŋa-Cruz, M. G. Montoya, and F. Manzano-Agugliaro, "Power quality techniques research worldwide: A review," *Renewable and Sustainable Energy Reviews*, vol. 54, pp. 846 – 856, 2016.

[3] V. Ansal, K. Ravikumar, and P. Parthiban, "Transformerless dynamic voltage restorer for voltage sag mitigation," in *Power and Energy Systems: Towards Sustainable Energy (PESTSE), 2016 Biennial International Conference on*. IEEE, 2016, pp. 1–4.

[4] M. Gayatri, A. M. Parimi, and A. P. Kumar, "Utilization of unified power quality conditioner for voltage sag/swell mitigation in microgrid," in *Power and Energy Systems: Towards Sustainable Energy (PESTSE), 2016 Biennial International Conference on*. IEEE, 2016, pp. 1–6.

[5] X. Zhang, G. Zhang, L. Jiang, and Z. Liu, "The research on solution of voltage interruption of network-side converter in dual-power emu," in *Proceedings of the 2015 International Conference on Electrical and Information Technologies for Rail Transportation*. Springer, 2016, pp. 113–122.

[6] N. A. Al-Emadi, C. Buccella, C. Cecati, and H. A. Khalid, "A novel dstatcom with 5-level chb architecture and selective harmonic mitigation algorithm," *Electric Power Systems Research*, vol. 130, pp. 251–258, 2016.

[7] A. El-Naggar and I. Erlich, "Control approach of three-phase grid connected pv inverters for voltage unbalance mitigation in low-voltage distribution grids," *IET Renewable Power Generation*, 2016.

[8] M. Gupta and A. Sindhu, "A novel technique for voltage flicker mitigation using dynamic voltage restorer," in *Proceedings of the International Congress on Information and Communication Technology*. Springer, 2016, pp. 273–281.

[9] D. Wei, W. Zhang, Z. J. Wang, and D. Zheng, "Study on improving microgrid transient power quality by super-capacitor," in *Advanced Materials Research*, vol. 960. Trans Tech Publ, 2014, pp. 845–848.

[10] J. Lin, Y. Sun, Y. Song, W. Gao, and P. Sorensen, "Wind power fluctuation smoothing controller based on risk assessment of grid frequency deviation in an isolated system," *IEEE Transactions on Sustainable Energy*, vol. 4, no. 2, pp. 379–392, 2013.

[11] S. K. Mondal, "Active and reactive power compensation of data center using multi-level statcom inverter," in *2016 IEEE 7th International Symposium on Power Electronics for Distributed Generation Systems (PEDG)*, June 2016, pp. 1–8.

[12] A. Marzoughi, H. Imaneini, and A. Moeini, "An optimal selective harmonic mitigation technique for high power converters," *International Journal of Electrical Power & Energy Systems*, vol. 49, pp. 34 – 39, 2013.

[13] M. Kesler and E. Ozdemir, "Synchronous-reference-frame-based control method for upqc under unbalanced and distorted load conditions," *IEEE Transactions on Industrial Electronics*, vol. 58, no. 9, pp. 3967–3975, Sept 2011.

[14] G. W. Chang, S. K. Chen, H. J. Su, and P. K. Wang, "Accurate assessment of harmonic and interharmonic currents generated by vsi-fed drives under unbalanced supply voltages," *IEEE Transactions on Power Delivery*, vol. 26, no. 2, pp. 1083–1091, April 2011.

[15] F. De la Rosa, *Harmonics and power systems*. CRC press, 2006.

[16] D. D. Shipp and W. S. Vilcheck, "Power quality and line considerations for variable speed ac drives," *IEEE Transactions on Industry Applications*, vol. 32, no. 2, pp. 403–410, 1996.

[17] Y.-J. Shin, E. J. Powers, M. Grady, and A. Arapostathis, "Power quality indices for transient disturbances," *IEEE Transactions on Power Delivery*, vol. 21, no. 1, pp. 253–261, 2006.

[18] W. G. Morsi and M. E. El-Hawary, "Defining power components in nonsinusoidal unbalanced polyphase systems: The issues," *IEEE Transactions on Power Delivery*, vol. 22, no. 4, pp. 2428–2438, Oct 2007.

[19] H. Kim, F. Blaabjerg, and B. Bak-Jensen, "Spectral analysis of instantaneous powers in single-phase and three-phase systems with use of pqr theory," *IEEE Transactions on Power Electronics*, vol. 17, no. 5, pp. 711–720, 2002.

[20] J. L. Blackburn, *Symmetrical components for power systems engineering*. CRC Press, 1993.

[21] D. Sharon, J.-C. Montano, A. Lopez, M. Castilla, D. Borras, and J. Gutierrez, "Power quality factor for networks supplying unbalanced nonlinear loads," *IEEE Transactions on Instrumentation and Measurement*, vol. 57, no. 6, pp. 1268–1274, 2008.

[22] B. Singh, A. Chandra, and K. Al-Haddad, *Power quality: problems and mitigation techniques*. John Wiley & Sons, 2014.

[23] M. Shwedhi and M. Sultan, "Power factor correction capacitors; essentials and cautions," in *Power Engineering Society Summer Meeting, 2000. IEEE*, vol. 3. IEEE, 2000, pp. 1317–1322.

[24] G. Deb, "Ferranti effect in transmission line," *International Journal of Electrical and Computer Engineering*, vol. 2, no. 4, p. 447, 2012.

[25] N. G. Hingorani and L. Gyugyi, *Understanding FACTS*. IEEE press, 2000.

[26] L. Czarnecki, S. M. Hsu, and G. Chen, "Adaptive balancing compensator [power system control]," *IEEE transactions on power delivery*, vol. 10, no. 3, pp. 1663–1669, 1995.

[27] H. A. Mohammadpour, A. Ghaderi, and E. Santi, "Analysis of sub-synchronous resonance in doubly-fed induction generator-based wind farms interfaced with gate–controlled series capacitor," *IET Generation, Transmission & Distribution*, vol. 8, no. 12, pp. 1998–2011, 2014.

[28] H. A. Mohammadpour, A. Ghaderi, H. Mohammadpour, and E. Santi, "{SSR} damping in wind farms using observed-state feedback control of {DFIG} converters," *Electric Power Systems Research*, vol. 123, pp. 57 – 66, 2015.

[29] L. Gyugyi, K. K. Sen, and C. D. Schauder, "The interline power flow controller concept: a new approach to power flow management in transmission systems," *IEEE transactions on power delivery*, vol. 14, no. 3, pp. 1115–1123, 1999.

[30] H. L. Ginn, "Comparison of applicability of power theories to switching compensator control," *Przegld Elektrotechniczny*, vol. 89, 2013.

[31] B. Singh, K. Al-Haddad, and A. Chandra, "A review of active filters for power quality improvement," *IEEE Transactions on Industrial Electronics*, vol. 46, no. 5, pp. 960–971, Oct 1999.

[32] S. Fryze, "Wirk-, blind-und scheinleistung in elektrischen stromkreisen mit nichtsinusförmigem verlauf von strom und spannung," *Elektrotechnische Zeitschrift, June*, no. 25, 1932.

[33] H. Akagi, Y. Kanazawa, and A. Nabae, "Instantaneous reactive power compensators comprising switching devices without energy storage components," *IEEE Transactions on Industry Applications*, vol. IA-20, no. 3, pp. 625–630, May 1984.

[34] H. Akagi, E. H. Watanabe, and M. Aredes, *Instantaneous power theory and applications to power conditioning*. John Wiley & Sons, 2007, vol. 31.

[35] E. Tedeschi, "Cooperative control of distributed compensation systems in electric networks under non-sinusoidal operations," 2009.

[36] L. S. Czarnecki, "Non-periodic currents: their properties, identification and compensation fundamentals," in *Power Engineering Society Summer Meeting, 2000. IEEE*, vol. 2. IEEE, 2000, pp. 971–976.

[37] L. Cohen, *Time-frequency analysis*. Prentice hall, 1995, vol. 778.

[38] B. Boashash, *Time-frequency signal analysis and processing: a comprehensive reference*. Academic Press, 2015.

[39] Y.-J. Shin, E. J. Powers, W. M. Grady, and A. Arapostathis, "Signal processing-based direction finder for transient capacitor switching disturbances," *IEEE Transactions on Power Delivery*, vol. 23, no. 4, pp. 2555–2562, 2008.

[40] S. Farghal, M. Kandil, and A. Elmitwally, "Evaluation of a shunt active power conditioner with a modified control scheme under nonperiodic conditions," *IEE Proceedings-Generation, Transmission and Distribution*, vol. 149, no. 6, pp. 726–732, 2002.

[41] L. S. Czarnecki and A. Lasicz, "Active, reactive, and scattered current in circuits with nonperiodic voltage of a finite energy," *Instrumentation and Measurement, IEEE Transactions on*, vol. 37, no. 3, pp. 398–402, 1988.

[42] L. M. Tolbert, Y. Xu, F. Z. Peng, J. Chen, and J. N. Chiasson, "Definitions for non-periodic current compensation," in *European Power Electronics Conference (EPE)*, 2003.

[43] A. Esfandiari, M. Parniani, and H. Mokhtari, "Power quality impacts of an electric arc furnace and its compensation," *Journal of Electrical Engineering & Technology*, vol. 1, no. 2, pp. 153–160, 2006.

[44] V. Staudt, "Fryze - buchholz - depenbrock: A time-domain power theory," in *Nonsinusoidal Currents and Compensation, 2008. ISNCC 2008. International School on*, June 2008, pp. 1–12.

[45] E. H. Watanabe and M. Aredes, "Compensation of nonperiodic currents using the instantaneous power theory," in *Power Engineering Society Summer Meeting, 2000. IEEE*, vol. 2. IEEE, 2000, pp. 994–999.

[46] E. H. Watanabe, H. Akagi, and M. Aredes, "Instantaneous p-q power theory for compensating nonsinusoidal systems," in *Nonsinusoidal Currents and Compensation, 2008. ISNCC 2008. International School on*, June 2008, pp. 1–10.

[47] H. Kim, F. Blaabjerg, B. Bak-Jensen, and J. Choi, "Instantaneous power compensation in three-phase systems by using pqr theory," *Power Electronics, IEEE Transactions on*, vol. 17, no. 5, pp. 701–710, 2002.

[48] Y. Xu, L. M. Tolbert, F. Z. Peng, J. N. Chiasson, and J. Chen, "Compensation-based nonactive power definition," *IEEE Power Electronics Letters*, vol. 1, no. 2, pp. 45–50, June 2003.

[49] H. Akagi, "Active filters and energy storage systems operated under non-periodic conditions," in *Power Engineering Society Summer Meeting, 2000. IEEE*, vol. 2, 2000, pp. 965–970 vol. 2.

[50] L. S. Czarnecki, "CurrentsâĂŹ physical components (cpc) concept: A fundamental of power theory," *Przeglad Elektrotechniczny*, vol. 84, no. 6, pp. 28–37, 2008.

[51] P. Salmeron and R. S. Herrera, "Distorted and unbalanced systems compensation within instantaneous reactive power framework," *IEEE Transactions on Power Delivery*, vol. 21, no. 3, pp. 1655–1662, July 2006.

[52] L. S. Czarnecki. Personal website-journal sectioni. [Online]. Available: http://www.lsczar.info/research/journals

[53] L. Czarnecki and G. Chen, "Compensation of semi-periodic currents," *European transactions on electrical power*, vol. 12, no. 1, pp. 33–39, 2002.

[54] A. Ghaderi, H. A. Mohammadpour, H. L. Ginn, and Y. J. Shin, "High-impedance fault detection in the distribution network using the time-frequency-based algorithm," *IEEE Transactions on Power Delivery*, vol. 30, no. 3, pp. 1260–1268, June 2015.

[55] M. Islam, H. A. Mohammadpour, A. Ghaderi, C. W. Brice, and Y.-J. Shin, "Time-frequency-based instantaneous power components for transient disturbances according to ieee standard 1459," *Power Delivery, IEEE Transactions on*, vol. 30, no. 3, pp. 1288–1297, 2015.

[56] A. Girgis, J. W. Stephens, E. B. Makram *et al.*, "Measurement and prediction of voltage flicker magnitude and frequency," *Power Delivery, IEEE Transactions on*, vol. 10, no. 3, pp. 1600–1605, 1995.

[57] H. L. Ginn, "Reference signal generators for distributed compensation," *Przegld Elektrotechniczny*, 2015.

[58] M. Savaghebi, J. C. Vasquez, A. Jalilian, J. M. Guerrero, and T.-L. Lee, "Selective compensation of voltage harmonics in grid-connected microgrids," *Mathematics and Computers in Simulation*, vol. 91, pp. 211–228, 2013.

[59] L. Meng, X. Zhao, F. Tang, M. Savaghebi, T. Dragicevic, J. C. Vasquez, and J. M. Guerrero, "Distributed voltage unbalance compensation in islanded microgrids by using a dynamic consensus algorithm," *IEEE Transactions on Power Electronics*, vol. 31, no. 1, pp. 827–838, Jan 2016.

[60] P. T. Cheng, C. A. Chen, T. L. Lee, and S. Y. Kuo, "A cooperative imbalance compensation method for distributed-generation interface converters," *IEEE Transactions on Industry Applications*, vol. 45, no. 2, pp. 805–815, March 2009.

[61] L. S. Czarnecki, "Scattered and reactive current, voltage, and power in circuits with nonsinusoidal waveforms and their compensation [power systems]," *IEEE Transactions on Instrumentation and Measurement*, vol. 40, no. 3, pp. 563–574, Jun 1991.

[62] L. Czarnecki, "Currents' physical components (cpc) concept: A fundamental of power theory," *Przegląd Elektrotechniczny*, vol. 84, pp. 28–37, 2008.

[63] H. L. Ginn III and G. Chen, "Flexible active compensator control for variable compensation objectives," *IEEE Transactions on Power Electronics*, vol. 23, no. 6, pp. 2931–2941, 2008.

[64] P. T. Cheng and T. L. Lee, "Distributed active filter systems (dafss): A new approach to power system harmonics," *IEEE Transactions on Industry Applications*, vol. 42, no. 5, pp. 1301–1309, Sept 2006.

[65] T.-L. Lee, P.-T. Cheng, H. Akagi, and H. Fujita, "A dynamic tuning method for distributed active filter systems," *IEEE Transactions on industry applications*, vol. 44, no. 2, pp. 612–623, 2008.

Appendix A

TFDI Convergence to the *THD* for Periodic Loads

This appendix is dedicated to demonstrate that the $TFDI$ converges to the THD when considering periodic quantities. Assume the current waveform contaminated with kth harmonic:

$$i(t) = sin(\omega_0 t) + \alpha \quad sin(k\omega_0 t) \tag{A.1}$$

where ω_0 is the fundamental frequency of the generated voltage (rad/s). It can be easily shown that the THD for such current waveform is $THD = \alpha\%$.

In the next step, assuming that the signals are transferred to the positive side of the frequency plane (such signals are known as analytical signals and are achieved using Hilbert transform of the original waveform), we can rewrite the equation (A.1) in the complex domain as follows:

$$i(t) = \quad e^{\omega_0 t} + \alpha \quad e^{k\omega_0 t} \tag{A.2}$$

As mentioned in [37], the Wigner-Ville distribution of a single sinusoid oscillating in frequency ω_0 with magnitude A is:

$$WVD(t, \omega) = A^2 \quad \delta(\omega - \omega_0) \tag{A.3}$$

It is also mentioned in the same reference that the summation of two signals $s(t) = s_1(t) + s_2(t)$ has the following Wigner-Ville Distribution:

$$WVD_s(t,\omega) = WVD_{s_1}(t,\omega) + WVD_{s_2}(t,\omega) + 2Re\{CWVD_{s_1+s_2}(t,\omega)\} \quad \text{(A.4)}$$

where Re denotes the real part of the signal, and CWVD denotes the cross Wigner-Ville distribution between two signals. Therefore, by concluding from equations (A.3) and (A.4), the Wigner-Ville distribution of the current waveform (equation (A.2)) is:

$$WVD_i(t,\omega) = \delta(\omega-\omega_0) + \alpha^2\delta(\omega-k\omega_0) + 2\alpha\delta(\omega-\frac{1}{2}(k+1)\omega_0)cos((k-1)\omega_0 t) \quad \text{(A.5)}$$

Now, the $TFDI$ will be calculated using the equation (2.7) as follows:

$$E_{s1} = \frac{1}{T}\int_{\omega_0-\varepsilon}^{\omega_0+\varepsilon}\int_0^T WVD_i(t,\omega)dtd\omega = \frac{1}{T} \quad \text{(A.6)}$$

$$E_s = \frac{1}{T}\int_0^{\omega_{max}}\int_0^T WVD_i(t,\omega)dtd\omega = \quad \frac{1+\alpha^2}{T} \quad \text{(A.7)}$$

$$TFDI_s = \sqrt{\frac{E_s - E_{s1}}{E_{s1}}} = \alpha\% \quad \text{(A.8)}$$

where ω_{max} is the highest frequency available in the signal.

Therefore, it is apparent that in the stationary condition, the TFDI converges to the THD. However, for the non-stationary condition, such as the one for non-periodic load current, the Fourier transform (therefore the THD) loses its meaning. On the contrary, the Wigner-Ville distribution stays valid in the case of non-stationarity. Therefore, the TFDI can replace the THD for the case of non-stationary current waveforms, e.g. non-periodic loads.

Now, the $TFDI$ will be calculated using the equation (2.7) as follows:

$$E_{s1} = \frac{1}{T}\int_{\omega_0-\varepsilon}^{\omega_0+\varepsilon}\int_0^T WVD_i(t,\omega)dtd\omega = \frac{1}{T} \tag{A.9}$$

$$E_s = \frac{1}{T}\int_0^{\omega_{max}}\int_0^T WVD_i(t,\omega)dtd\omega = \quad \frac{1+\alpha^2}{T} \tag{A.10}$$

$$TFDI_s = \sqrt{\frac{E_s - E_{s1}}{E_{s1}}} = \alpha\% \tag{A.11}$$

where ω_{max} is the highest frequency available in the signal.

Therefore, it is apparent that in the stationary condition, the TFDI converges to the THD. However, for the non-stationary condition, such as the one for non-periodic load current, the Fourier transform (therefore the THD) loses its meaning. On the contrary, the Wigner-Ville distribution stays effective in the case of non-stationarity. Therefore, the TFDI is able to replace the THD for the case of non-stationary current waveforms, e.g. non-periodic loads.

Appendix B

Proof of Equation (3.18)

This section is dedicated to the mathematical explanation of the equation Part I-(3.18). Assume that the single phase instantaneous voltage at the terminal of the non-periodic load consists of odd harmonics, and the single phase instantaneous current of the non-periodic load consists of both odd harmonics and low frequency modulating odd harmonics:

$$v(t) = \sum_{n=1}^{\infty} V_n cos(n\omega_0 t) \tag{B.1}$$

$$i(t) = \sum_{n=1}^{\infty} \sum_{m=1}^{\infty} I_{(n,m)} cos((n\omega_0 \pm m\Delta\omega)t - \phi_{(n,m)}) \tag{B.2}$$

where n is the order of existing harmonics in the current and voltage (odd numbers for power system), and m is the order of existing harmonics in the modulating signal (odd numbers for regular modulating signal), $\Delta\omega(= 2\pi f_m)$ is the modulation frequency, and ω_0 is the power system frequency.

The equivalent conductance of the load is calculated using equation Part I-(3.15). In this equation the denominator is always constant, assuming the calculation window (T) is an integer multiple of the power system frequency period ($T = lT_0$). Therefore, in order to reach the compensation goal, which is absence oscillating component in the equivalent conductance, the nominator of equation Part I-(3.15) should be kept constant. This is possible, only if T is an integer multiple of all the period of all frequency components of $p(t)$ in equation (B.3).

Using equation (B.1), and (B.2) the components of $p(t)$ for each phase are calcu-

lated as follows:

$$\begin{aligned} p(t) &= v(t)i(t) \\ &= \sum_{n=1}^{\infty}\sum_{m=1}^{\infty} P_{(n,m)}cos(n\omega_0 t)cos(L\omega_0 t - \phi_{(n,m)}) \end{aligned} \tag{B.3}$$

where $P_{(n,m)} = V_n I_{(n,m)}$, $L = n \pm mk$ and k is the modulation ratio ($k = \frac{\Delta\omega}{\omega_0}$). From the trigonometric product-to-sum identity, $p_{(n,m)}(t)$ could be rewritten as:

$$p_{(n,m)}(t) = \frac{P_{(n,m)}}{2}[cos(L'\omega_0 t - \phi_{(n,m)}) + cos(L''\omega_0 t + \phi_{(n,m)})] \tag{B.4}$$

where $L' = n + L = 2n \pm mk$ and $L'' = n - L = \mp mk$ are the frequency orders (multiplication of ω_0) available in the instantaneous power ($p(t)$) waveform. Therefore, assuming zero $\phi_{(n,m)}$ to simplify the calculation, the value of the oscillating part of the average power ($\widetilde{P}$, which corresponds to the oscillating part of the equivalent conductance) can be calculated using equation (B.3) as follows:

$$\widetilde{P} = \sum_{n=1}^{\infty}\sum_{m=1}^{\infty} \frac{P_{(n,m)}}{2T}[\frac{sin(L'\omega_0 T)}{L'\omega_0} + \frac{sin(L''\omega_0 T)}{L''\omega_0}] \tag{B.5}$$

Therefore, by replacing T with lT_0 (which means $\omega_0 T = 2\pi l$), and replacing L' with $2n \pm mk$ and L'' with $\mp mk$, the oscillating part of the power is equal to:

$$\widetilde{P} = \sum_{n=1}^{\infty}\sum_{m=1}^{\infty} P_{(n,m)}[K'\frac{sin(\pm 2\pi lmk)}{l} + K''\frac{sin(\mp 2\pi lmk)}{l}] \tag{B.6}$$

where $K' = \frac{1}{4\pi L'}$ and $K'' = \frac{1}{4\pi L''}$.

Therefore, it can be concluded that the oscillating part of the equivalent conductance has a double relationship with the window length (l) with the following equation:

$$\widetilde{G}_e \quad \propto \quad \frac{sin(\pm 2\pi lmk)}{l} \tag{B.7}$$

Therefore, there are two options for achieving equivalent conductance with small oscillation, a gigantic window length, or a window length that keeps the lmk product

close to an integer value ($sin(integer \times \pi) = 0$). It should be noted that, since there is more than one modulating harmonic, it is desired that the oscillation of high power modulating harmonics (high $P_{(n,m)}$) is decreased more compared to modulating harmonics with lower power. In other words, the lmk product should be much closer to an integer for higher $P_{(n,m)}$. This significance of the stronger oscillating components is reflected in the fuzzy rules of the proposed algorithm.

Appendix C

C-code Demonstration

In this appendix, a c-code example of the slow compensator is provided. This code is the part of the code that runs inside the infinite loop ($while(1)$). Note that to build a minimal program, several components are not mentioned in this section, including, service interrupt routines, preprocessors, error checking and error issuing functions, read and write functions, functions for communication with the host, and multi-threading commands.

```
// variable definition
static double vt,it;//voltage and current
static double ps,P=1,v2s,Ge=0;
static double Vp2=1;//voltage squared
static double  read_array[2];//read data
static double pa [1801]; //instantaneous power of size NT+1= fs*T+1 =1801
static double v2a [1801]; //instantaneous voltage squared of size NT+1= fs*T+1 =1801
static unsigned short counter=0; //for switching to recursive calculation
static unsigned short k; //recursive loop counter
static double  p_end,p_beg,delP;// for recursive loop calculation
static double  v2_end,v2_beg,delV2;// for recursive loop calculation
static double iG=0; //compensating current
//infinite loop
while(1) {
GetAnalogInput(read_array); //function to receive voltage and current samples
it=read_array[0];//getting current sample
vt=read_array[1];//getting voltage sample
ps=it*vt; //instantaneous power
v2s=vt*vt;//instantaneous voltage squared
//for recursive calculation (refer to equations (41) and (42)
p_beg=pa[1800];//NT
p_end=pa[0];
delP=p_end-p_beg;
```

```
v2_beg=v2a[/*N*/1800];
v2_end=v2a[0];
delV2=v2_end-v2_beg;
//first the calculation is performed using non-recursive
//integrals to achieve the steady state value of the integral
if (counter<2000) {
counter++;
//calculation of the power average using non-recursive technique
P=pa[0];
Vp2=v2a[0];
for (k= 1800-1; k > 0; k--){
P+= pa[k];
pa[k]=pa[k-1]; // this loop is also used to shift
// the arrays to make place for new samples
Vp2+= v2a[k];
v2a[k]=v2a[k-1];
}
}
//recursive calculation
else if (counter>=2000){ // once the average reached a steady
// state value the recursive calculation starts
for (k=1801-1; k > 0; k--){// this loop is used to shift the arrays
// to make place for new samples
pa[k]=pa[k-1];
v2a[k]=v2a[k-1];
}
P+=delP ;//recursive calculation of power
Vp2+=delV2 ;//recursive calculation of squared voltage
}
//loading the new value into arrays
pa[0]= ps;
v2a[0]=v2s;
//calculating the output current
Ge=P/(Vp2);
iG=it-Ge*vt;//current reference calculation
//writing the current value on analog output
WriteAnalogInput(iG); //function to write the reference generating current
}
```

Appendix D

Non-periodic Current Modeling

As discussed previously, the non-periodic current demonstrates some form of amplitude modulation with a fixed modulation frequency. Therefore, a technique is proposed in this work for simple modeling the non-periodic load current which based on the amplitude modulation observation. In this appendix, this model is developed and formulated. Current waveform of the load is the amplitude modulation of a carrier with a modulating waveform:

$$i_L = (1 + m(t))c(t) \tag{D.1}$$

where $i_L(t)$ is the load current, $m(t)$ is modulating waveform, and $c(t)$ is the carrier waveform. The modulating waveform is calculated using the following equation:

$$m(t) = m_0 \; tri(\omega_m t) \tag{D.2}$$

where m_0 is modulation amplitude, tri is the triangle waveform, and ω_m is the modulating frequency in rad/s. The carrier waveform is calculated as follows:

$$c_0(t) = A_1 sin(\omega_0 t - \phi_0) + A_3 sin(3\omega_0 t - 3\phi_0) \tag{D.3}$$

$$c(t) = \begin{cases} c_0(t) & if \quad |c_0(t)| > th \\ 0 & otherwise \end{cases} \tag{D.4}$$

where th set the threshold so that the current waveform demonstrates the sharp edges. Please note that when this current is generated using the load emulator, the slope of

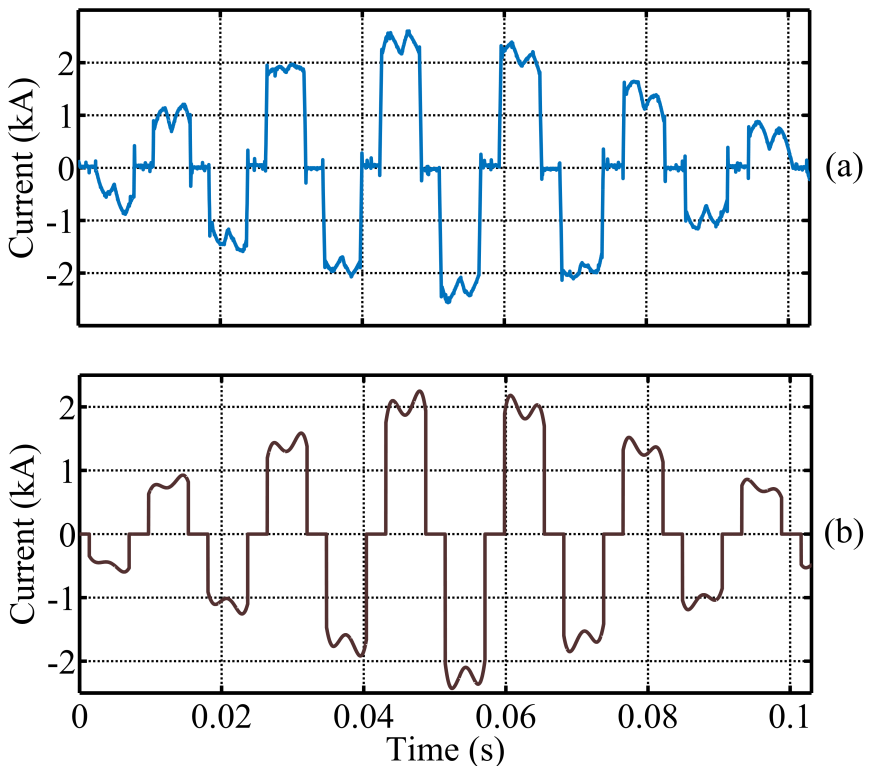

Figure D.1: (a) Real-world current waveform (*loading case* 4), (b) current waveform resulted from the proposed modeling technique.

the sharp edges will be dictated by the slew rate of the analog output device.

Fig.D.1 compares the result of the proposed model and the real-world data current waveform (*loading case* 4). It is evident that by neglecting the environmental noise, the proposed model of the current waveform converges to the real-world current waveform. To achieve this model, the following values are used: $m_0 = 0.75$, $\omega_m = 58.81 rad/s$, $A_1 = 1.6$, $A_3 = 0.5$, $\omega_0 = 376.3 rad/s$, $th = 1.5$.